

Review

# Recent Advances in Organic Radicals and Their Magnetism

Sharvan Kumar, Yogendra Kumar, Sudhir Kumar Keshri and Pritam Mukhopadhyay \*

Supramolecular and Material Chemistry Lab, School of Physical Sciences, Jawaharlal Nehru University, New Delhi 110067, India; shravan.aug12@gmail.com (S.K.); ykchem007@gmail.com (Y.K.); skjnu2011@gmail.com (S.K.K.)

\* Correspondence: m\_pritam@mail.jnu.ac.in or pritam.jnu@gmail.com; Tel.: +91-011-2673-8772

Academic Editor: Floriana Tuna

Received: 5 October 2016; Accepted: 22 November 2016; Published: 30 November 2016

**Abstract:** The review presents an overview of the organic radicals that have been designed and synthesized recently, and their magnetic properties are discussed. The  $\pi$ -conjugated organic radicals such as phenalenyl systems, functionalized nitronyl nitroxides, benzotriazinyl, bithiazolyl, aminyl-based radicals and polyradicals, and Tetrathiafulvalene (TTF)-based H-bonded radicals have been considered. The examples show that weak supramolecular interactions play a major role in modulating the ferromagnetic and antiferromagnetic properties. The new emerging direction of zethrenes, organic polyradicals, and macrocyclic polyradicals with their attractive and discrete architectures has been deliberated. The magnetic studies delineate the singlet-triplet transitions and their corresponding energies in these organic radicals. We have also made an attempt to collate the major organic neutral radicals, radical ions and radical zwitterions that have emerged over the last century.

**Keywords:** organic radicals; biradicals and polyradicals; magnetism; supramolecular interactions; self-assembly

## 1. Introduction

Organic molecules we frequently come across in our daily lives are comprised of closed-shell electronic structures with equal numbers of electrons with up- and down-spins. Therefore, most organic compounds are diamagnetic [1]. The paradigm-shifting discovery of the triphenylmethyl radical [2] by Moses Gomberg in 1900 was a major landmark in the 20th century, which set the stage for studies of molecules with unpaired electrons, i.e., systems with open-shell electronic structures. After this discovery, several classes of organic radical systems having one or more unpaired electrons have been synthesized [3]. These radical systems can be polyradicals, biradicals and diradicals. In the biradicals, the distance between the two unpaired electrons in the molecule is too large and the electron exchange interaction ( $J$ ) between them is negligible or nearly negligible [4,5]. On the other hand, when, in a molecule comprised of two unpaired electrons, the magnitude of the dipole-dipole interaction is large enough to produce two spin states, i.e., singlet and triplet, it is referred to as a diradical [4,6]. These novel organic radical systems have initiated a wide range of highly interesting applications in redox-catalysis [7,8], living radical polymerization [9–11] and particularly magnetochemistry [12,13], the topic which pertains to this review. In addition, radicals find new-age applications as components in batteries [14,15], molecular spintronics [16], and the kondo effect [17], as well as in chemical biology and medicine as spin-labeling agents, in electron paramagnetic resonance (EPR) imaging and also in the diverse areas of biochemistry [18,19].

The design of pure all-organic molecular materials with magnetic properties has been one of the challenges of the last few decades. In this context, the indispensable work of Cambi and Szego

on spin-crossover magnetic materials in 1930 [20] has been one of the essential reference points for chemists, physicists and materials scientists towards the generation of pure organic magnetic materials. In the pure organic compounds, as a result of the constituent light-weight elements, only the isotropic magnetic exchange interactions govern the magnetic behavior at temperatures above 0.1 K. The other magnetic interactions in organic radical systems, for example hyperfine or spin-orbit interactions, sources of magnetic anisotropies, are believed to be insignificant above this temperature. As a consequence, magnetic organic systems are described at zero applied magnetic field by the effective spin Hamiltonian approach by  $H = -2 \sum J_{ij} S_i S_j$  (1), where  $S_{ij}$  represents the effective exchange interaction parameter for the magnetic centers  $i$  and  $j$ , having total quantum spin numbers  $S_i$  and  $S_j$ , respectively, with the summation operating over the adjacent pair of centers. From eqn. (1), when  $S_{ij}$  is positive the magnetic interaction is ferromagnetic (FM), and if  $S_{ij}$  is negative the interaction is antiferromagnetic (AFM). In general, organic magnetic materials exhibit paramagnetic properties at high temperatures. The three aspects central to designing organic molecular materials with bulk magnetic properties which should be diligently considered are: (i) the permanence of the spin-containing moieties; (ii) the magnetic interaction mechanism or the coupling routes between the neighboring spin-possessing moieties; and (iii) the transmission of the magnetic interactions along the material [21]. Based on the different possibilities of the coupling routes, a FM interaction may originate if an orthogonal organization with a zero overall overlap integral between the two singly-occupied molecular orbitals (SOMOs) of the two interacting moieties is produced. In contrast, an AFM interaction results if such an integral is non-zero for non-degenerate orbitals. Magnetic interactions can take place in an intramolecular fashion between two (or more) spin-containing units within the same molecule, or in an intermolecular fashion between organic radicals governed by the isotropic exchange interactions between the unpaired electrons of the nearest molecules positioned on the respective SOMOs. Therefore, the creation of organic magnetic materials would require control over supramolecular interactions within the spin-containing sub-units, in order to promote the correct isotropic exchange interactions between the adjacent organic radicals. Supramolecular interactions such as hydrogen bonding,  $\pi$ - $\pi$  stacking, halogen bonding [22] and bridging of radical ions through the counter-ions are the majorly applied non-covalent intermolecular interactions to assemble such molecular building blocks.

In one of the earliest reports on an organic ferromagnet, Tamura et al. in 1991 reported the existence of FM intermolecular interactions in the crystals of *p*-nitrophenyl-nitronyl nitroxide [23], with a ferromagnetically ordered state below 0.65 K. After this pioneering report, diverse design strategies were applied towards the goal of realizing ferromagnetically ordered organic free radicals at the highest possible temperature. The result that has remained unsurpassed to date is a sulfur-nitrogen-based organic radical with a magnetic ordering at 36 K [24].

We have collated a list of diverse organic neutral radicals [25–71], radical anions [72–104], radical cations [105–131] and zwitterionic radicals [132–136] in Charts 1–3 according to the year of their report. It is to be noted that the list is not exhaustive. The goal has been to acquaint the reader with different classes of radicals that have emerged over time and to illustrate the growing interest towards creation of new organic radicals. Several of these radicals have been isolated and structural characterization has been carried out. Innovative design principles have led to radicals with unprecedented ambient stabilization and also a handful of radicals that can withstand even the acidic chromatography matrix during their purification. Also of tremendous interest to the synthetic radical chemistry community is to improve their opto-electronic properties, having the potential to exhibit multistability. Several of the radicals and radical ions outlined in Charts 1–3 have found tremendous applications as organic magnetic molecular materials. After presenting the collection of organic radicals, we have considered the recent (2011 until now) advances made in the design and magnetic studies of  $\pi$ -conjugated organic radicals such as phenalenyl systems, nitronyl nitroxides, benzotriazinyl, bisthiazolyl, aminyl-based radicals and polyradicals, and H-bonded Tetrathiafulvalene (TTF)-based radicals (Sections 2–7). The examples clearly show that weak noncovalent interactions play a major role in modulating

ferromagnetic and antiferromagnetic properties. We have also deliberated on the emerging direction of organic radicals based on polycyclic aromatic hydrocarbons, i.e., zethrenes, organic polyradicals and macrocyclic polyradicals (Section 8).

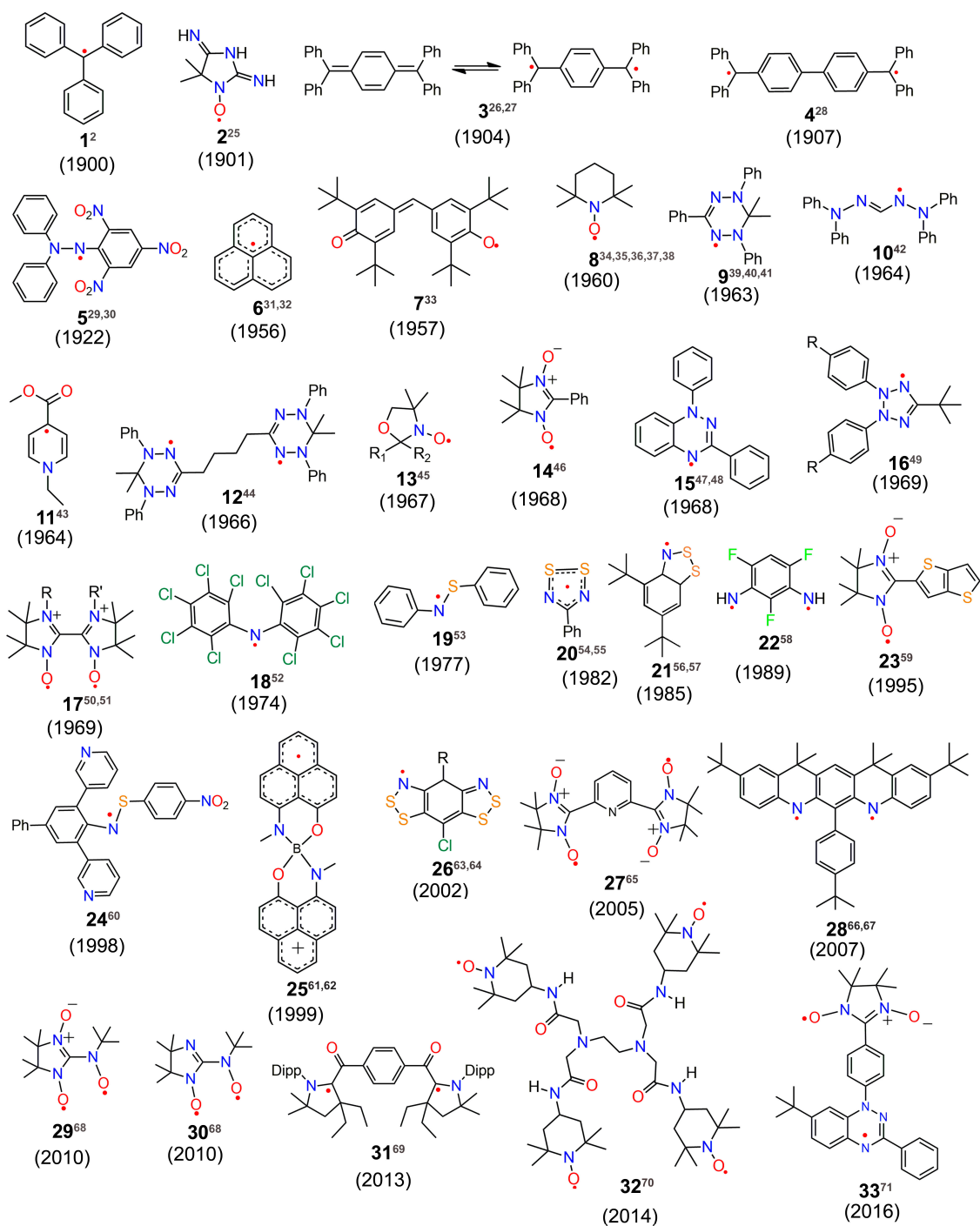


Chart 1. Molecular structures of organic neutral radicals.

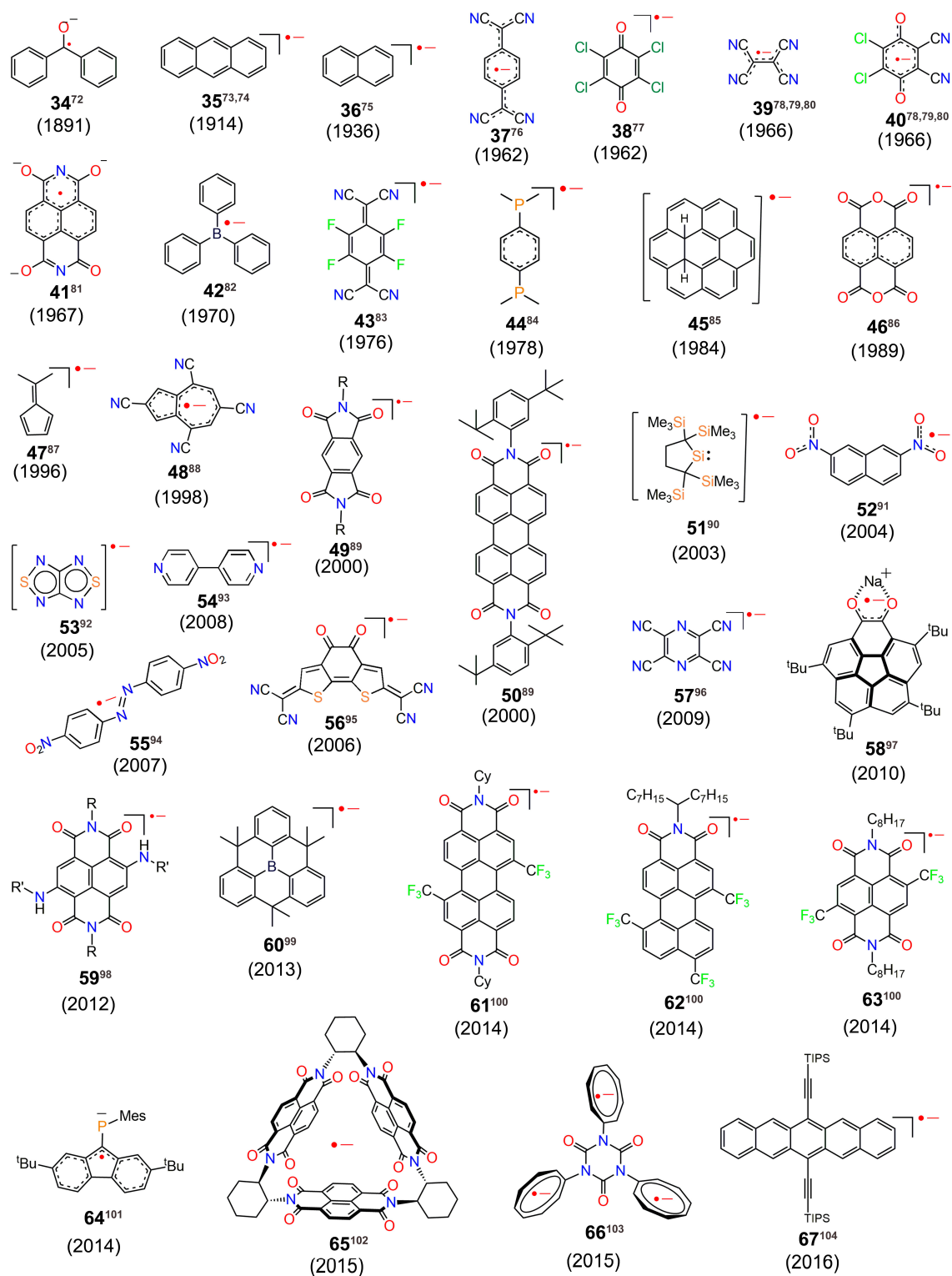


Chart 2. Molecular structures of organic radical ions.

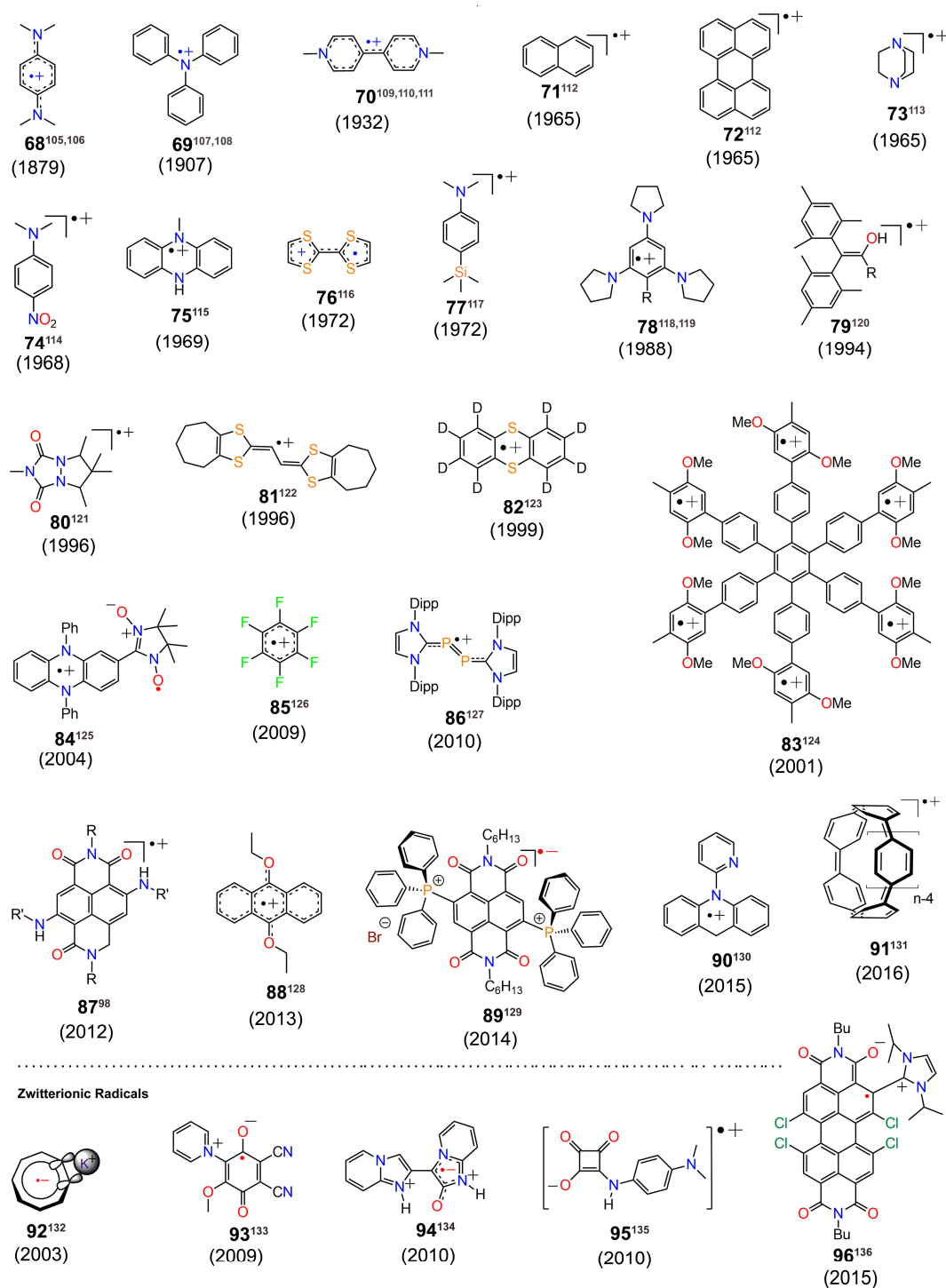
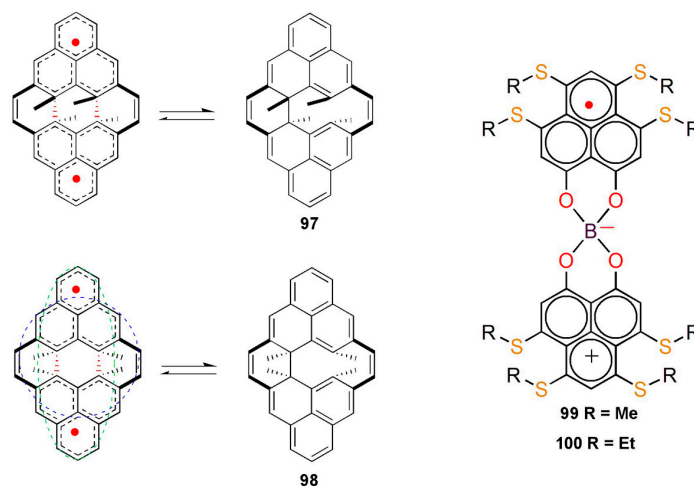


Chart 3. Molecular structures of organic radical cations and zwitterionic radicals.

## 2. Phenalenyl-Based $\pi$ -Radical

The phenalenyl (PLY)  $\pi$ -radical **6** is a stable hydrocarbon radical known for the last several decades [31]. The stability of **6** arises from the  $\pi$ -electron delocalization of the unpaired electron; however, **6** could not be isolated due to its  $\sigma$ -dimerization. Various PLY-based organic molecular materials have been designed and synthesized, prompting experimental and theoretical studies due to their intriguing opto-electronic and magnetic properties. The fascinating properties emerge from the ability of phenalenyl and its derivatives to form  $\pi$ -dimers in addition to  $\sigma$ -dimers. Huang et al. have

reported a paramagnetic cyclo-biphenalenyl biradicaloid with chair (97) and boat conformations (98) (Figure 1a) [137]. The paramagnetism emerges from the triplet of the  $\pi$ -dimer as the singlet states are magnetically silent.



**Figure 1.** Left column depicts the valence tautomerizations between  $\pi$ -dimers and right column shows the valence tautomerizations between the  $\sigma$ -dimers of the chair 97 and boat conformations 98 of the cyclo-biphenalenyl biradicaloid molecule. The  $2e/mc$  (multi-centered)  $\pi$ - $\pi$  bondings are represented by the red/green/blue dashed lines/curves. The hydrogen atoms have been removed for clarity. Reproduced from Reference [137]. Copyright 2011 American Chemical Society. And the molecular structure of 99 and 100.

Haddon et al. have reported synthetically intricate PLYs based on the spiro-bis(3,4,6,7-tetrachalcogenide-substituted phenalenyl) boron salts and the corresponding tetrathiomethyl (99)- and tetrathioethyl (100)-substituted spiro-bis(phenalenyl)boron radicals having the PLY nucleus substituted [138]. The radicals 99 and 100 existed as weak  $\pi$ -dimers in the solid state due to steric encumbrance of the thioalkyl groups in the overlaid PLY units.

Magnetic susceptibility measurements of radicals 99 and 100 determined the paramagnetic components of the magnetic susceptibility. For both radicals, the  $\chi_P$  follows the Curie-Weiss behavior,  $\chi_P = C / (T - \theta)$  and Curie constants  $C$  corresponding to 0.291 and 0.366 emu/mol, respectively, were determined (Figure 2a). The negative Weiss constants  $\theta$  of  $-4.0$  and  $-8.0$  K of radicals 99 and 100, respectively, and the reduced spin counts realized at low temperatures pointed towards the AFM interactions concomitant to the dimeric character of the radicals (Figure 2b).

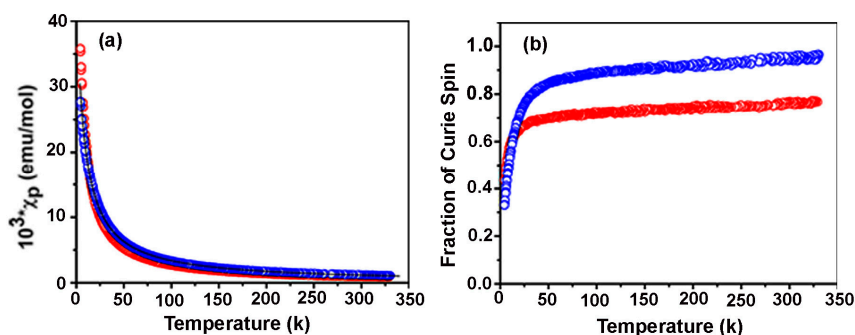


**Figure 2.** (a) Plots of the magnetic susceptibilities of 99 (red) and 100 (blue). Note the black line representing the Curie-Weiss fit of the magnetic data for 100; (b) Fraction of Curie spins obtained from  $\chi T$  for 99 (red) and 100 (blue). Reproduced from Reference [138]. Copyright 2013 American Chemical Society.

### 3. Nitronylnitroxides

A diverse range of organic nitronylnitroxide-based molecules has been synthesized and their magnetic properties have been well studied by several groups. We will discuss some recent examples, which have been designed based on subtle functional group modifications, for example aminophenylnitronylnitroxides, hydroxyphenylnitronylnitroxides and biphenyl nitronylnitroxides.

#### 3.1. Aminophenylnitronylnitroxides

Aminophenylnitronylnitroxides comprise two N-H-based H-bond donors, which form prevalent hydrogen-bonding interactions in their N-H crystal lattices. Lahti et al. have reported the synthesis and magnetic properties of 2-(*para*-aminophenyl)-4,4,5,5-tetramethyl-4,5-dihydro-1H-imidazole-3-oxide-1-oxyl (*p*APN) (**101**) and 2-(*meta*-aminophenyl)-4,4,5,5-tetramethyl-4,5-dihydro-1H-imidazole-3-oxide-1-oxyl (*m*APN) (**102**) (Chart 4) [139]. The intermolecular contacts, with effective spin orbital overlap between high-spin-density nitronylnitroxide sites involving the N–O units, result in strong magnetic exchange interactions. Compound **102** exhibited a Curie constant of  $C = 0.368 \text{ emu}\cdot\text{K}/\text{Oe}\cdot\text{mol}$ , and a substantially large AFM Weiss constant of  $\theta = -36.2 \text{ K}$  (Figure 3a). A maximum at 40–50 K was revealed from the  $\chi$  versus  $T$  plot, which is characteristic of the AFM exchange (Figure 3b).

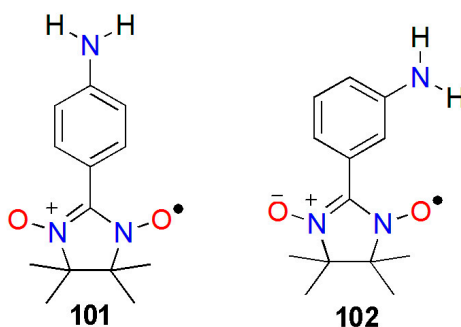
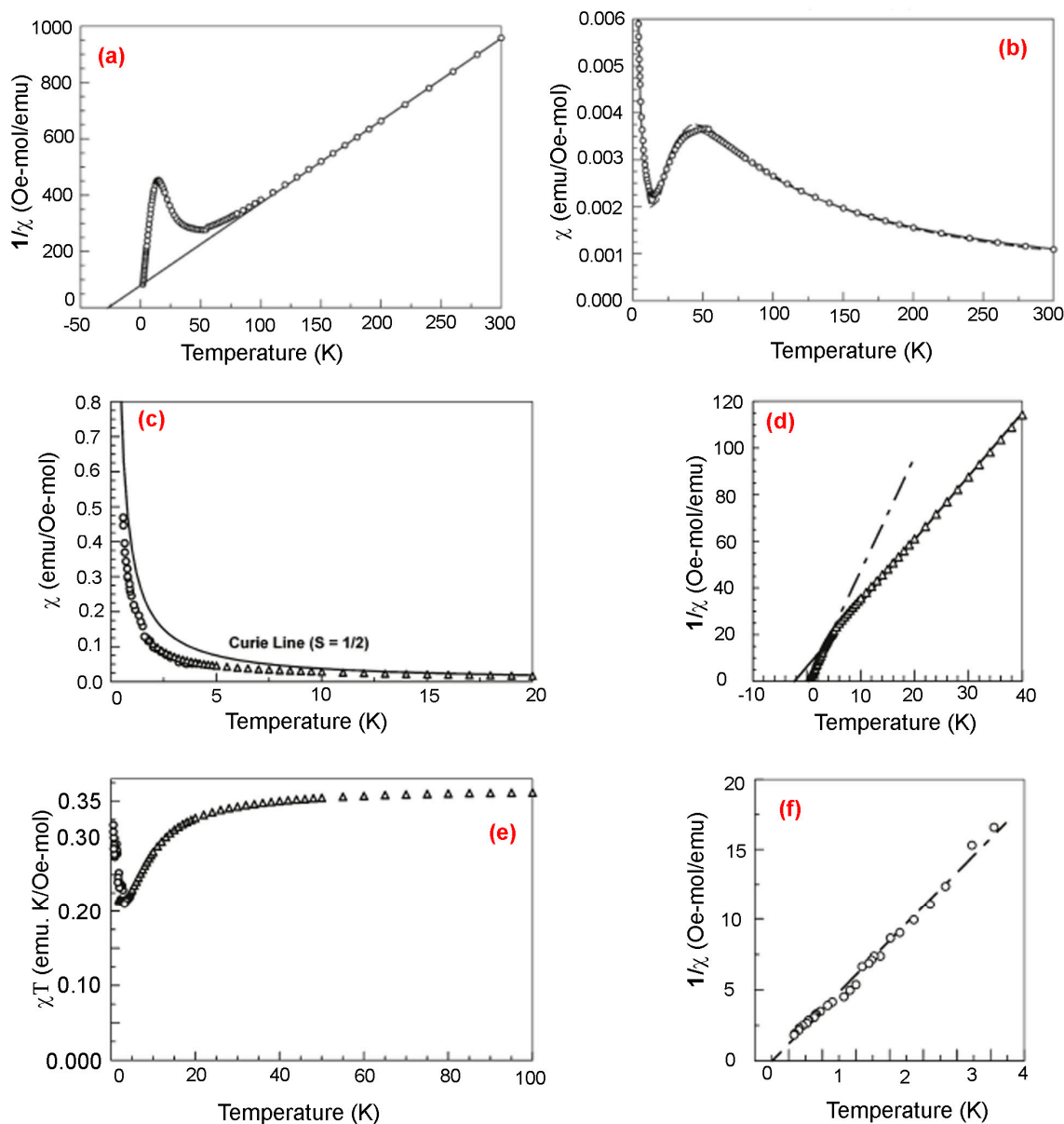


Chart 4. Molecular structures of **101** and **102**.

The AFM exchange interaction could be revealed as the  $\chi$  versus  $T$  data for **101** was positioned below the paramagnetic Curie curve (Figure 3c). The higher temperature region of the  $1/\chi$  versus  $T$  plot demonstrated a Curie constant of  $0.363 \text{ emu}\cdot\text{K}/\text{Oe}\cdot\text{mol}$ , and an extrapolated Weiss constant  $\theta = -3.4 \text{ K}$  having an alteration of the slope at about 5 K (Figure 3d). The AFM interactions at the higher temperature region were also established in the  $\chi T$  versus  $T$  plot, which decreased considerably in the range 50–3 K (Figure 3e). However, at 2–3 K the decrease levels out, and therefore, the susceptibility behavior has been investigated in the range of 0.3–3.6 K (Figure 3f). Interestingly, competing exchange pathways were revealed in **101** as  $\chi T$  versus  $T$  increased after minimizing at about 2 K. A small positive Weiss constant of  $+0.26 \text{ K}$  with a Curie constant of  $0.2 \text{ emu}\cdot\text{K}/\text{Oe}\cdot\text{mol}$  could be determined from the  $1/\chi$  versus  $T$  plot of the 0.6–3.6 K data.



**Figure 3.** Plots for the paramagnetic susceptibility data of **102**: (a)  $1/\chi$  vs.  $T$  plot linearly fitted and (b)  $\chi$  vs.  $T$  fitted with without meanfield (broken line) and including mean field (solid line) the data was acquired using the 1000 Oe external field. Paramagnetic susceptibility data for **101**: (c)  $\chi$  vs.  $T$  plot; with noninteracting spin curie line (d)  $1/\chi$  vs.  $T$  plot depicting linear fits to data at higher (solid line) and lower (broken line) temperature regions: (e)  $\chi T$  vs.  $T$  plot; and (f) low temperature  $1/\chi$  vs.  $T$  plot depicting the linear fit to data. The data obtained at  $T > 1.8$  K at 1000 Oe are shown in triangles and the data collected by ac-susceptibility with zero field at  $0.6$  K  $< T < 4$  K are shown with circles. Reproduced from Reference [139]. Copyright 2011, American Chemical Society.

### 3.2. Hydroxyphenylnitronylnitroxides

Lahti et al. reported the synthesis of 2-(3',5'-dimethoxy-4'-hydroxyphenyl)-4,4,5,5-tetramethyl-4,5-dihydro-1H-imidazole-1-oxyl (**103**), also called "syringylnitronylnitroxide" (SyrNNO) [140] (Figure 4). X-ray crystallography results clearly established inter-radical close contacts formed by O-H...O and C-H...O types of H-bonds (Figure 4).

The plot of the molar magnetization ( $M/M_s$ ) versus field ( $H$ ) (Figure 5a) for **103** showed a normalization to an expected field-saturated magnetization of 5585 emu/mol for  $S = 1/2$  spin carriers.

The  $M/M_s$  plot rests below the Brillouin curve as anticipated for isolated  $S = 1/2$  spins, indicating significant intermolecular AFM exchange interactions.  $M/M_s$  vs.  $H$  is fairly linear up to 40,000 Oe at 2.0 K with a very subtle inflection point at  $\sim 7000$  Oe. In contrast, at 0.55 K the  $M/M_s$  vs.  $H$  exhibited a concave down-region from 1000 to 7000 Oe, and a concave up-region from 7000 to 40,000 Oe, as clearly seen from Figure 5a. This state is followed by a concave down-region above 40,000 Oe and finally saturation around  $\sim 50,000$  Oe.

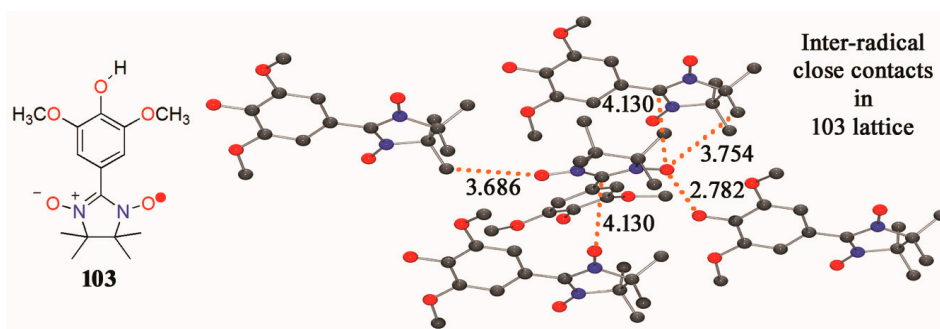


**Figure 4.** Structure of **103** and supramolecular interactions involving the SyrNN nitronyl nitroxide units in **103**: 2D network formation through hydrogen-bonded OH...O–N chains, inter-radical N–O...C chain contacts, and radical methyl CH...ON interactions. H atoms have been removed for clarity. Reproduced from Reference [140]. Copyright 2013, American Chemical Society.

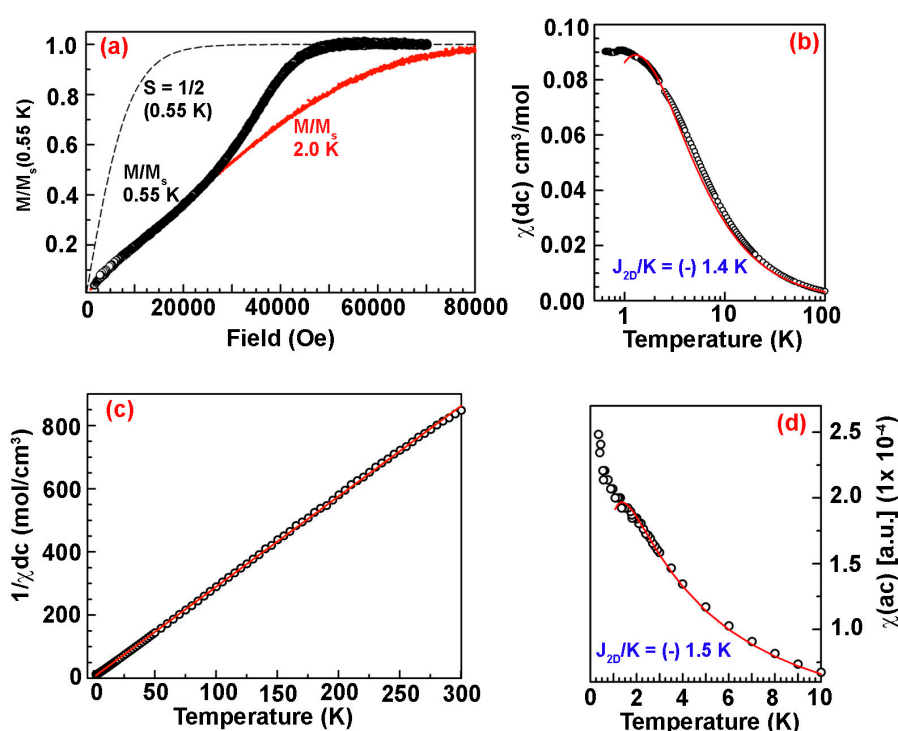


**Figure 5.** (a) Plot of molar magnetization normalized to saturation magnetization ( $M/M_s$ ) versus field at 0.55 K (upper, black data) and 2.0 K (lower, red data). The Brillouin curve for isolated  $S = 1/2$  spins at 0.55 K and magnetic susceptibility versus temperature is depicted by the dashed lines; (b) Plot of  $\chi_{dc}$  versus  $T$  at 1000 Oe external field; (c) Plot of  $1/\chi_{dc}$  versus  $T$  data in zero external field (modulation 10 Oe, frequency 155 Hz); and (d) shows  $\chi_{ac}$  versus  $T$  data in zero external field (modulation 10 Oe, frequency 155 Hz). The solid red lines exhibits fits to an AFM 2D square planar model without mean field correction. Reproduced from Reference [140]. Copyright 2013, American Chemical Society.

The  $\chi_{dc}$  versus  $T$  curve persists below the Curie curve, again indicating AFM exchange (Figure 5b). Furthermore, AFM exchange was also revealed from the Curie–Weiss plot of  $1/\chi_{dc}$  versus  $T$ , which produced a Weiss constant of  $\theta = -1.4$  K (Figure 5c). The plot rises below 4 K monotonically and levels out below 1.5 K to give an ill-defined maximum at about 0.9 K. A zero field ac susceptibility plot over 0.35–10 K exhibited  $\chi_{ac}$  versus  $T$  to rise below 4 K, as is also shown in Figure 5d. There is no indication that **103** forms a magnetically ordered state above 0.35 K since no maximum in the zero field  $\chi_{ac}$  versus  $T$  plot could be delineated.

### 3.3. Biphenyl-4,4'-bis(nitronylnitroxide)

Baumgarten et al. have described the strong AFM interactions in biphenyl-4,4'-bis(nitronylnitroxide) (**104**) (Chart 5) in solution as well as in the solid state [141]. The strength of the AFM intra-dimer coupling constant was found to be  $J/k_B = -14.0 \pm 0.9$  K. In addition, a magnetic field-induced transition for the field distinctly above 20 T was suggested from the inter-dimer coupling  $J'/k_B$  at 1 K, which is contingent on the topology of the magnetic couplings.

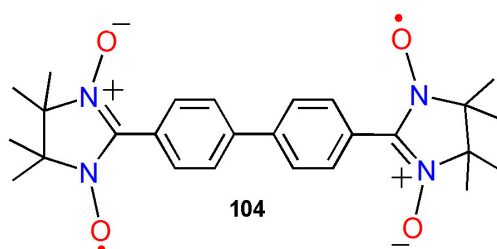
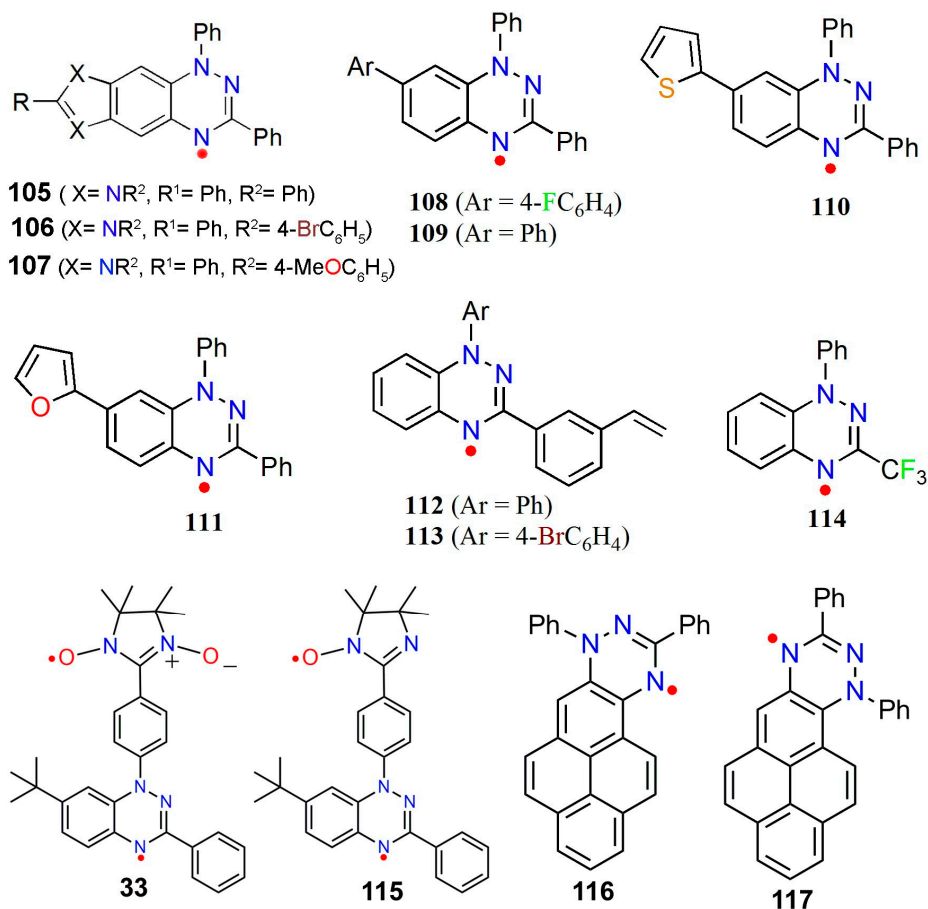


Chart 5. Molecular structure of **104**.

## 4. Benzotriazinyl Radicals

The 1,2,4-benzotriazin-4-yls were first reported by Blatter et al. in the late 1960s [47]. Koutentis et al. have reported the synthesis of a series of imidazo-, oxazo-, and thiazolo-fused 1,2,4-benzotriazinyls and deliberated on the dimensionality of the magnetic interactions of these systems. This group studied the magneto-structural correlations based on variable-temperature (VT) studies of 1,3,7,8-tetraphenyl-4,8-dihydro-1H-imidazolo [1,2,4] benzotriazin-4-yl (**105**), 8-(4-bromophenyl)-1,3,7-triphenyl-4,8-dihydro-1H-imidazolo [1,2,4] benzotriazin-4-yl (**106**), and 8-(4-methoxyphenyl)-1,3,7-triphenyl-4,8-dihydro-1H-imidazolo[1,2,4] benzotriazin-4-yl (**107**) (Chart 6) [142].



**Chart 6.** Representative radicals of 1,2,4-benzotriazinyl.

The molar susceptibility ( $\chi$ ) for the radicals **105** and **106** increased gradually upon cooling from 300 K and reached a broad maximum at  $T_{max} = (50 \pm 2)$  and  $(50 \pm 4)$  K, respectively, which indicated strong antiferromagnetic interactions (Figure 6a,b). Further,  $\chi$  decreased gradually down to 15 K for **105** and to 20 K for **106** before it increased subsequently at lower temperatures. The uncoupled radicals at defect sites in the lattice were thought to be responsible for this increase in  $\chi$  at low temperatures. On the other hand, **107** displayed different a magnetic behavior as it followed Curie-Weiss behavior between 5 and 300 K with  $C = 0.338 \text{ emu}\cdot\text{K}\cdot\text{mol}^{-1}$  close to the value expected for  $S = 1/2$  spin (Figure 6c). The positive Weiss constant of 1.83 K indicated the presence of local FM interactions between the radicals. Upon lowering the temperature from 300 K,  $\chi T$  increased and attained a maximum at  $T_{max} = (30 \pm 4)$  K. Below this temperature,  $\chi T$  fell sharply, suggesting the presence of AFM interactions at low temperatures.

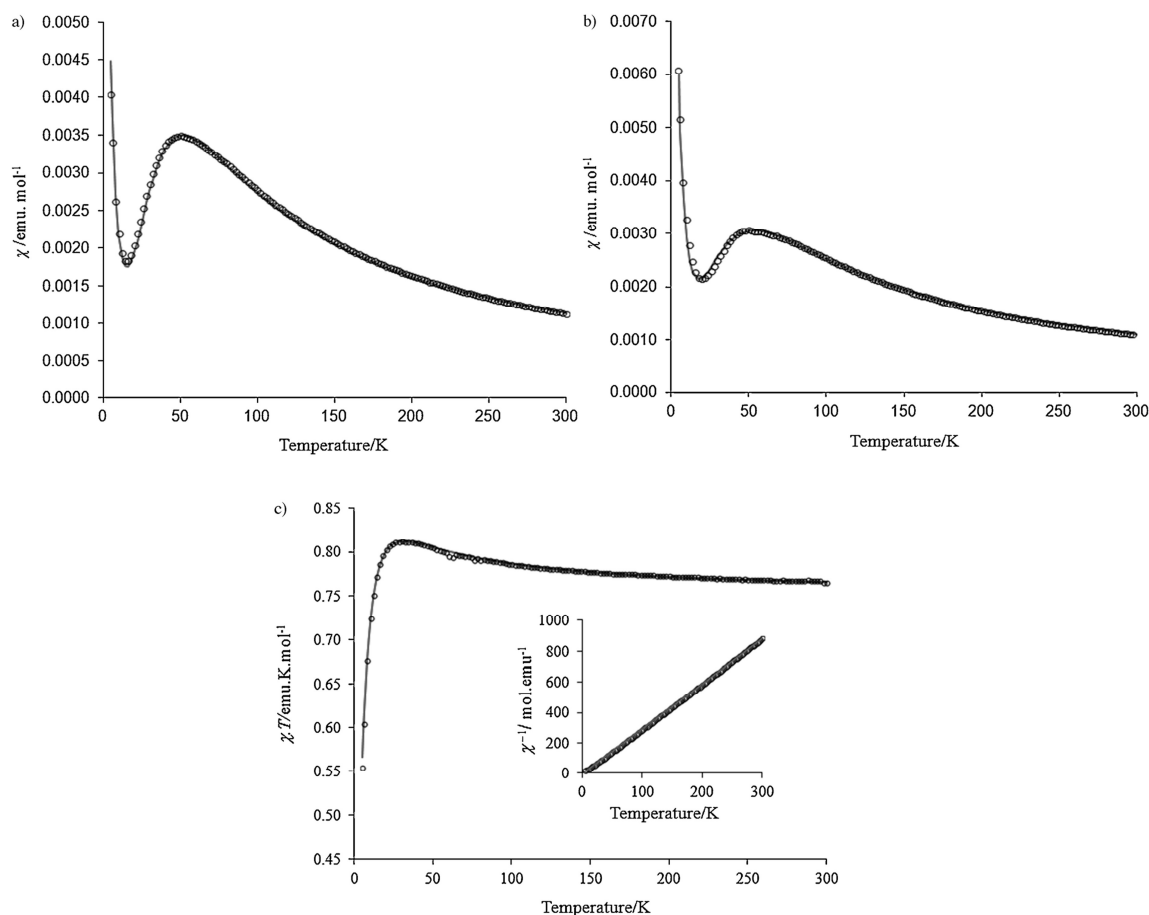


**Figure 6.** Plot of  $\chi$  versus  $T$  for radicals (a) **105**, (b) **106** and (c) plot of  $\chi T$  versus  $T$  and (inset)  $1/\chi$  versus  $T$  for radical **107**. (a) The solid line signifies the best fit to the 1D alternating AF linear chain model for  $S = 1/2$  spin;  $J = -31.3 \text{ cm}^{-1}$ ,  $\alpha = 0.15$ ,  $\rho = 0.94$ ,  $g_{\text{solid}} = 2.0030$ ,  $R = 5.82 \times 10^{-4}$ ; (b) The solid line signifies the best fit to the 1D alternating AF linear chain model for  $S = 1/2$  spin;  $J = -35.4 \text{ cm}^{-1}$ ,  $\alpha = 0.38$ ,  $\rho = 0.91$ ,  $g_{\text{solid}} = 2.0028$ ,  $R = 7.58 \times 10^{-4}$ ; (c) The solid line shows the best fit to the Bleaney–Bowers model for a pair of interacting  $S = 1/2$  spins with  $2J = 23.6 \text{ cm}^{-1}$ ,  $2zJ' = -2.8 \text{ cm}^{-1}$ ,  $g_{\text{solid}} = 2.0028$ ,  $R = 6.55 \times 10^{-4}$ . Inset depicts the Curie-Weiss behavior in the 5–300 K region,  $C = 0.338 \text{ emu}\cdot\text{K}\cdot\text{mol}^{-1}$  and  $\theta = 1.83 \text{ K}$ . Reproduced with permission from Reference [142]. Copyright 2014, Wiley-VCH.

Koutentis et al. reported the synthesis and AFM interactions in the 1D Heisenberg linear chains of 1,3-diphenyl-7-(4-fluorophenyl)-1,4-dihydro-1,2,4-benzotriazin-4-yl (**108**) and 1,3-diphenyl-7-phenyl-1,4-dihydro-1,2,4-benzotriazin-4-yl (**109**) (Chart 6) [143]. The  $\pi$ -backbone of the benzotriazinyl radical coupled with the 1D,  $\pi$ -slipped stacked columns of radicals **108** and **109** directs strong uni-dimensional magnetic interactions propagating parallel to the stacking direction (Figure 7a,b). This is since the overlap between singly-occupied molecular orbitals is maximized parallel to the stacking direction. Radical **108** established Curie-Weiss behavior above 50 K with  $C = 0.374 \text{ emu}\cdot\text{K}\cdot\text{mol}^{-1}$  and a Weiss constant of  $\theta = -11.3 \text{ K}$ , which is consistent with the local AFM interactions. Radical **109** showed similar magnetic behavior to that of radical **108** (Figure 7c,d).

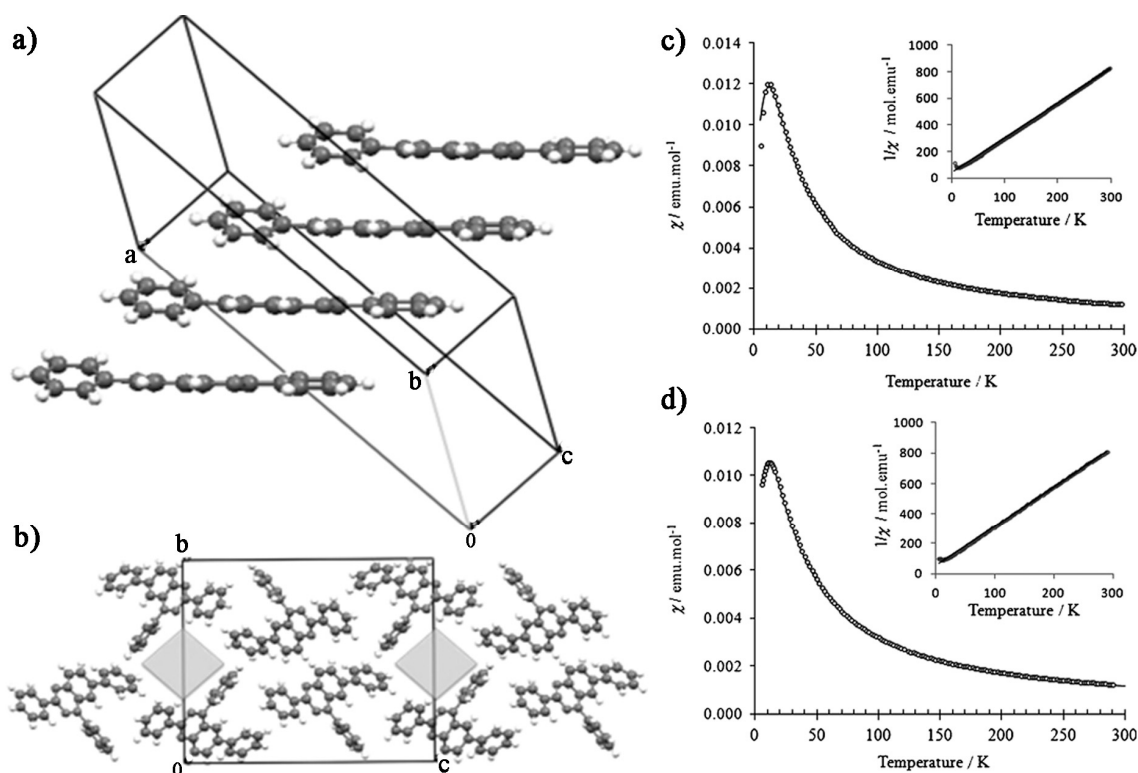


**Figure 7.** Packing of **109**. (a) The  $\pi$ -stacks of radicals along the c-axis (N-phenyls have been removed for clarity); (b) Antiparallel chains along the a-axis form voids as depicted by grey boxes. Plot of  $\chi$  versus  $T$  for radicals **108** (c) and **109** (d). The solid line denotes the best fit to the 1D AFM regular linear chain model. For radical **108**,  $J = -12.9 \text{ cm}^{-1}$ ,  $zJ' = -0.4 \text{ cm}^{-1}$ ,  $g = 2.0069$ ; For radical **109**,  $J = -11.8 \text{ cm}^{-1}$ ,  $zJ' = -6.5 \text{ cm}^{-1}$ ,  $g = 2.0071$ . Inset shows the Curie-Weiss behavior in the 50–300 K region,  $C = 0.374 \text{ emu}\cdot\text{K}\cdot\text{mol}^{-1}$ ,  $\theta = -11.3 \text{ K}$  for **108** and  $C = 0.379 \text{ emu}\cdot\text{K}\cdot\text{mol}^{-1}$ ,  $\theta = -19.2 \text{ K}$  for **109**. Reproduced with permission from Reference [143]. Copyright 2012, Wiley-VCH.

This group further reported the synthesis of  $\pi$ -stacked 1,3-diphenyl-7-(thien-2-yl)-1,4-dihydro-1,2,4-benzotriazin-4-yl (**110**) and the FM interactions of 1D linear chains [144]. Compound **110** adopted a glided  $\pi$ -stacked structure of centrosymmetric dimers with alternate short and long interplanar distances of 3.48 Å and 3.52 Å, respectively. Magnetic susceptibility measurements revealed that **110** followed Curie-Weiss behavior in the 5–300 K region with  $C = 0.378 \text{ emu}\cdot\text{K}\cdot\text{mol}^{-1}$  and  $\theta = +4.72 \text{ K}$ . This result is consistent with the FM interactions between  $S = 1/2$  radicals.

Subsequently, Koutentis et al. reported the first example of a thermally accessible triplet state from a benzotriazinyl radical. They reported the synthesis of 1,3-diphenyl-7-(fur-2-yl)-1,4-dihydro-1,2,4-benzotriazin-4-yl (**111**) [145]. Importantly, solid-state VT-EPR spectroscopy of (**111**) between 5 and 140 K established the triplet exciton ( $|D| = 0.018 \text{ cm}^{-1}$ ,  $|E| = 0.001 \text{ cm}^{-1}$ ). Theoretical studies based on DFT calculations and SQUID measurements revealed strong temperature dependence of the magnetic exchange interaction within the dimer building block.

Frank et al. reported the synthesis of 1-phenyl-3-(3-vinylphenyl)-1,2,4-benzotriazin-4-yl (**112**)- and 1-(4-bromophenyl)-3-(3-vinylphenyl)-1,2,4-benzotriazin-4-yl (**113**)-based radicals with low oxidation potential and FM interactions [146]. They found out that the radicals **112** and **113** produce glided 1D  $\pi$ -stacks due to the  $\pi$ - $\pi$  interaction, which results in intra-chain FM and inter-chain AFM exchange interactions leading to metamagnetic behavior. In the 50–300 K temperature range, the magnetic susceptibility for both the radicals obeyed Curie-Weiss behavior to give Weiss constants of  $\theta = +4.0$  (**112**) and  $\theta = +3.7 \text{ K}$  (**113**) in coherence with the prevailing FM interactions.

In a significant development, Koutentis et al. reported the synthesis of 1-phenyl-3-trifluoromethyl-1,4-dihydrobenzo[e]-[1,2,4]triazin-4-yl (**114**) [147], and it is the first example of a hydrazyl radical that demonstrates a reversible sharp spin transition between a paramagnetic and a diamagnetic phase at 58(2) K. Notably, this transition is completed within a slender temperature range of 5(1) K. The first-order transition proceeds via small changes in the intra- and inter-stack interactions between comparable structural phases. X-ray crystallography demonstrated clear changes in the intermolecular interactions at 4 K and 75 K (Figure 8). This offers significant future potential to use different stimuli to drive such phase changes.

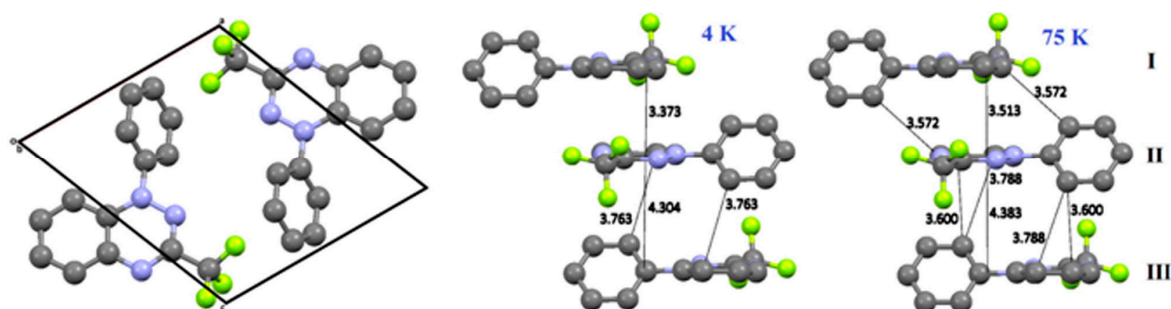


**Figure 8.** A view of the unit cell of **114** down the b-axis (left) and  $\pi$ -stacks of **114** at 4 K (middle) and depiction of the supramolecular contacts and the interplanar distances in pairs I–II and II–III at 75 K (right). H atoms have been removed for clarity. Reproduced from Reference [147]. Copyright 2014, American Chemical Society.

Recently, Rajca et al. reported Blatter radicals, which are based on high-spin diradicals **33** and **115** [71]. Diradical **33** is thermally stable up to  $\sim 175$  °C under inert conditions, and it sublimes at 140 °C under high vacuum without decomposition. However, radical **115** start decomposition at  $\sim 75$  °C. The advantage of these radicals is that the spin density is delocalized over the N1 phenyl of the 1,2,4-benzotriazenyl radical. This induces ferromagnetic interactions through the trimethylenemethane (TMM)-like ferromagnetic coupling of the nitronyl/imino nitroxides. The low temperature (139–147 K) electron paramagnetic resonance (EPR) spectra of 1.3 mM diradical **33** and 0.4 mM diradical **115** in frozen glasses (toluene/ $\text{CHCl}_3$  4:1) show unresolved hyperfine coupling to five non-equivalent nitrogens.

Casu et al. reported the synthesis of radical **116** [148]. During the synthesis they considered two possible constitutional isomers, **116** and **117**, due to the two different modes of fusing pyrene and Blatter radicals: 1,3-diphenyl-1,4-dihydro-1,2,4-triazin-4-yl. The DFT calculation showed significant out-of-plane twisting in the pyrene moiety and high energy in the constitutional isomer **117**; thus, they selected **116**. The EPR spectrum of **116** in benzene at room temperature showed hyperfine coupling.

## 5. Bis-Dithiazolyl Radicals

The first thiazolyl radical was reported in 1985 by R. Mayer [56,57]. Thiazyl-based neutral radicals are highly interesting since the sulfur heteroatom augments intermolecular magnetic and electronic interactions. Among them, the radicals based on the pyridine-bridged bis-dithiazolyl framework are remarkable molecular constructs as their solid-state structures as well as their transport properties can be modulated by varying the peripheral ligands or by the replacement of sulfur by selenium. Oakley et al. have also reported the bis-diselenazolyl radicals by simple replacement of S by its heavier Se analogue. They have prepared a series of isostructural S/Se-containing variants (Chart 7: 118–121) [149].

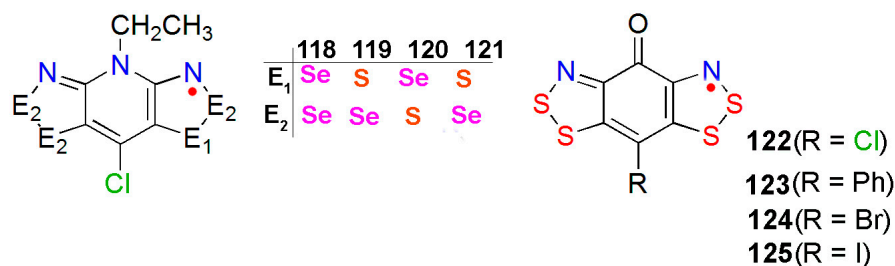


**Chart 7.** Molecular structures of bis-dithiazolyl radical molecules.

Interestingly, all the radicals were found to crystallize in non-centric space groups (Figure 9). The structures comprised of pinwheel-like clusters of radicals arranged about four centers, with each of the four radicals within the pinwheel offering the foundation for a glided,  $\pi$ -stacked arrangement running parallel to the  $c$ -axis. They compared the magnetic properties of the bis-diselenazolyl radical (118) with its isostructural 119, 120 and 121 radicals using the ferromagnetic absorption method. The experimental data of bis-diselenazolyl radical 118 confirmed the commencement of the long-range FM order below  $T_C$ , as well as a remarkably large coercive field,  $H_C$ , which was revealed by this organic ferromagnet.

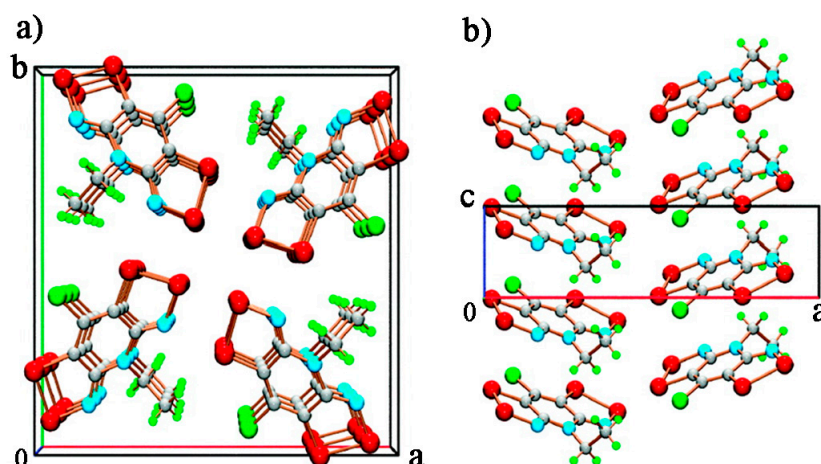


**Figure 9.** A view of the crystal packing of 118: (a) Parallel and (b) perpendicular to the  $\pi$ -stacking direction. Radicals 119, 120, and 121 were found to be isostructural to 118. Reproduced from Reference [149]. Copyright 2011, American Chemical Society.

Oakley et al. have subsequently reported a range of semiquinone-bridged bis-dithiazolyl radicals and studied their conductive and magnetic properties. They reported the variable-temperature (VT) magnetic susceptibility of acetonitrile solvates 122 [150] and 123 [151] (Chart 7). Compounds 119 and 120 constitute a novel class of  $\pi$ -radicals for use in the design of  $S = 1/2$  conductors.

A strong AFM-coupled paramagnetic behavior could be established from the cooling curve plots of  $\chi$  and  $\chi T$  versus  $T$  for solvated 122 (Figure 10a,b), which was measured using an external field of  $H = 1$  kOe [150]. Remarkably, a large negative  $\theta$  value of  $-61.7$  K was realized from the Curie–Weiss fit over the range 100–300 K. However, there was no substantiation for a structural or magnetic phase transition upon cooling the sample to 2 K. The high-temperature cooling curve data (with  $H = 1$  kOe) for the unsolvated material 122 (Figure 10c,d) also suggested an AFM-coupled Curie–Weiss paramagnet with  $\theta = -27.0$  K. On the other hand, upon cooling below 10 K, this magnetic material demonstrated a sharp increase in  $\chi$  as well as  $\chi T$ .

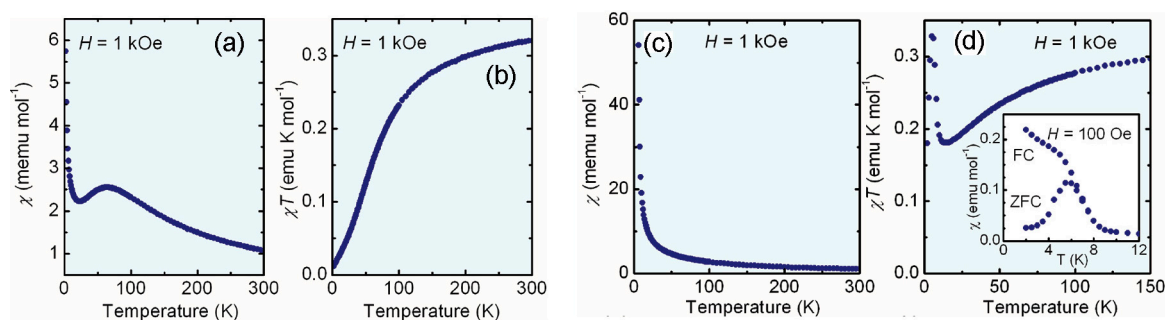


**Figure 10.** (a) A plot of field-cooled,  $\chi$  versus  $T$ ; and (b)  $\chi T$  versus  $T$  for solvated **122** at  $H = 1$  kOe; (c) Plot of field-cooled  $\chi$  versus  $T$  for unsolvated **122** at  $H = 1$  kOe; (d) Field-cooled  $\chi T$  versus  $T$  plot for unsolvated **122** at  $H = 1$  kOe. Inset depicts a ZFC/FC plot of  $\chi$  versus  $T$  at  $H = 100$  Oe. Reproduced from Reference [150]. Copyright 2011, American Chemical Society.

The crystal structure of **123** belonged to a non-centric space group and was comprised of sheets of nearly coplanar radicals intermolecularly fastened together by a series of supramolecular  $S3 \cdots O'$  contacts (2.858 Å) (Figure 11a) [151]. These sheets with alternating ABABAB  $\pi$ -stacks were constituted of adjacent radicals, which are related by the two-fold screw axis along the  $x$  direction (Figure 11b,c). The closest neighbors along the  $\pi$ -stacks are separated by  $S1 \cdots S3'$  contacts with  $d_1$  (3.680 Å) and  $d_2$  (3.806 Å), which are slightly larger than the sum of the  $S \cdots S'$  van der Waals radii. The field-cooled  $\chi T$  versus  $T$  plot for radical **123** at a field  $H = 1$  kOe (Figure 12a) was suggestive of paramagnetic behavior, with strong local FM coupling along the  $\pi$ -stacks. A Curie-Weiss fit to the data above 100 K afforded  $C = 0.349$  emu·K·mol<sup>-1</sup>. Investigation of the data over the range  $T = 6$ –30 K for a Heisenberg 1D FM-coupled  $\pi$ -stacked chain of  $S = 1/2$  centers generated exchange coupling constants  $J = +29.5$  cm<sup>-1</sup> for interactions along the  $\pi$ -stacks and  $zJ' = -2.5$  cm<sup>-1</sup> for the inter-stack interactions. A consequent zero field cooled-field cooled (ZFC-FC) experiment at  $H = 100$  Oe revealed a phase transition at 4.5 K. The resulting state can be regarded in terms of spin-canted AFM ordering based on the antiparallel alignment of the FM-coupled  $\pi$ -stacked chains.

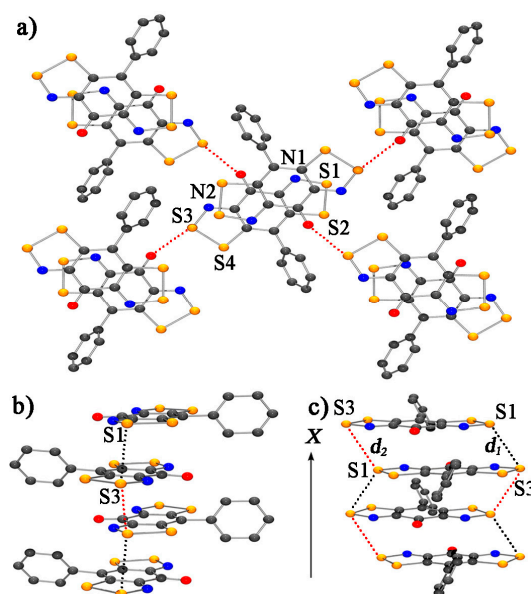


**Figure 11.** (a) A view of the unit cell of **123**, viewed perpendicular to the  $yz$  plane, with intermolecular  $S3 \cdots O'$  supramolecular contacts depicted with dashed lines; (b,c) Views of the ABABAB  $\pi$ -stacks in **120**, with  $S1 \cdots S3$  contacts  $d_1$  and  $d_2$ . Reproduced with permission from Reference [151]. Copyright 2011, the Royal Society of Chemistry.

Further, Oakley et al. have also reported the Br- and I-derivatives of bis-dithiazolyl radicals **124** and **125** [152]. The field-cooled variable-temperature (2–300 K)  $\chi T$  versus  $T$  measurements for **125** at  $H = 1$  kOe (Figure 12b) revealed strong FM exchange interactions. This was indicated by a  $\theta$  value of +23.3 K obtained from a Curie-Weiss fit to the 100–300 K data. Upon cooling below 90 K, the subsequent decrease in  $\chi T$  signaled the onset of weaker AFM interactions leading to spin-canted antiferromagnetic ordering below  $T_N = 35$  K, as revealed by bifurcation in  $\chi T$  for the ZFC and FC sweeps.

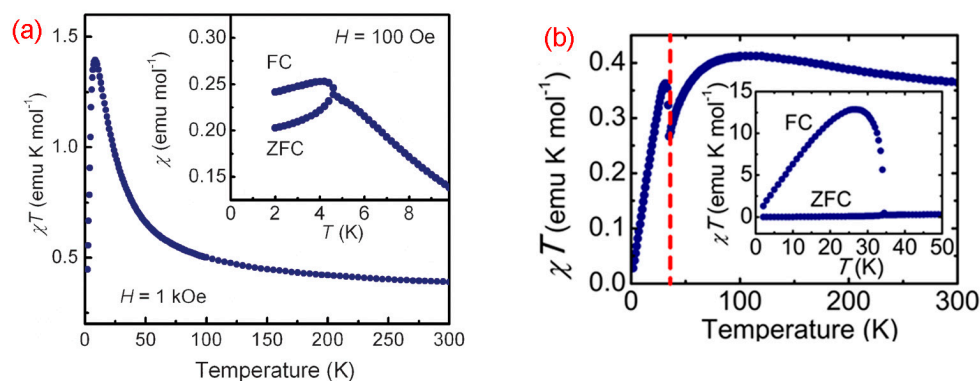


**Figure 12.** (a) The  $\chi T$  vs.  $T$  plot for **123** at  $H = 1$  kOe. Inset exhibits ZFC-FC plots of  $\chi$  vs.  $T$  at  $H = 100$  Oe. Reproduced with permission from Reference [151]. Copyright 2011, the Royal Society of Chemistry; (b) Field-cooled  $\chi T$  vs.  $T$  plot for **125**, at  $H = 1$  kOe. Inset shows the ZFC-FC plot of  $\chi T$  vs.  $T$  at  $H = 10$  Oe. Reproduced from Reference [152]. Copyright 2015, American Chemical Society.

## 6. Aminyl Radicals

### 6.1. Aminyl Diradicals

The nitrogen-centered aminyl-based radicals are typically short-lived, and only a handful of aminyl monoradicals are stable under ambient conditions. Recently, Rajca et al. have reported the synthesis and magnetic characterization of sterically shielded aminyl diradical **126**, which possessed a triplet ground state with a  $\Delta E_{S-T}$  comparable to that of *m*-xylylene **127** (Chart 8) [67]. However, **126** was found to be persistent in solution at room temperature on the time scale of minutes. The triplet ground state for **126** was unambiguously confirmed by SQUID magnetometry as verified by the  $S = 1$  paramagnetic behavior for both  $M$  as a function of  $H$  as well as the plot of  $\chi$  versus  $T$  (Figure 13). A small AFM coupling due to weak intermolecular interactions in solutions of **126** was suggested based on the mean-field parameter  $\theta \approx -0.2$  K. Notably; this is the first example of an organic diradical that is persistent in solution at room temperature up to minutes with a singlet-triplet energy gap of 10 kcal/mol.

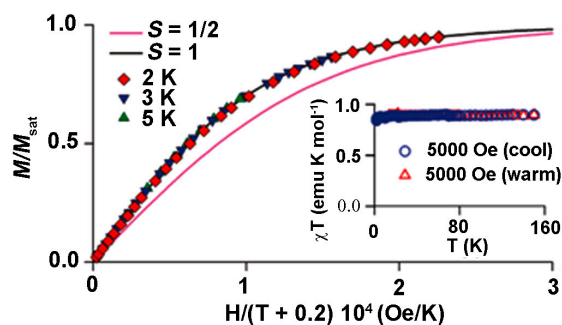


**Figure 13.** A plot of  $M/M_{sat}$  vs.  $H/(T - \theta)$  from the SQUID magnetometry data of **126** in 2-Me THF (20 mM). Inset shows a plot of  $\chi T$  vs.  $T$ .  $\theta = -0.2$  K,  $M_{sat} = 0.89$   $\mu$ B,  $S = 1.0$ , and  $\chi T = 0.89$   $\text{emu} \cdot \text{K} \cdot \text{mol}^{-1}$ . Reproduced from Reference [67]. Copyright 2011, American Chemical Society.

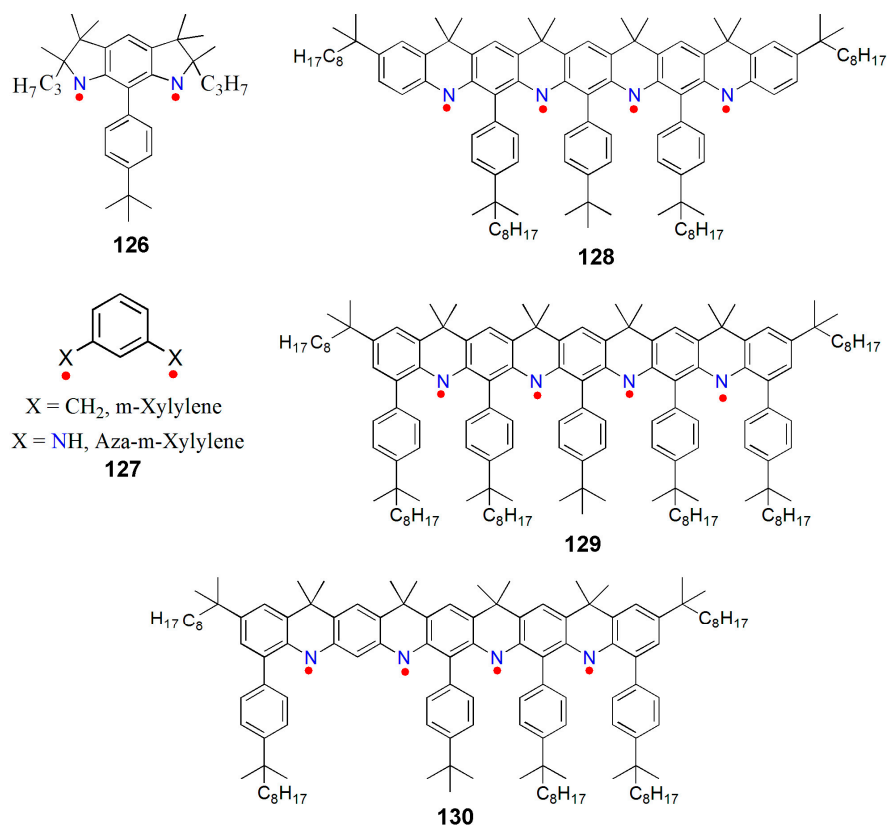


**Chart 8.** Molecular structures of aminyl diradicals and tetraradicals.

### 6.2. Aminyl Tetraradicals

Rajca et al. also reported a series of aminyltetraradicals, **128–130**, and their magnetic properties (Figure 14) [153]. In **125–127**, an effective  $2p\pi-2p\pi$  overlap within the  $\pi$ -system of aminyl radicals and m-phenylenes was possible as a result of the planarity of the tetraazononacene backbone. A quintet ( $S = 2$ ) ground state could be established separated from the low spin-excited states by an energy gap of  $\Delta E \sim 5 \text{ kcal}\cdot\text{mol}^{-1}$ . Interestingly, the carbon and nitrogen atoms with predominant spin densities are sterically shielded, which enhanced the stability of the tetraradicals without disturbing the planarity of the radical system. The tetraradical **129** possessed five 4-tert-alkylphenyl steric groups, and in 2-methyltetrahydrofuran at room temperature it possessed a half-life of 1 h.

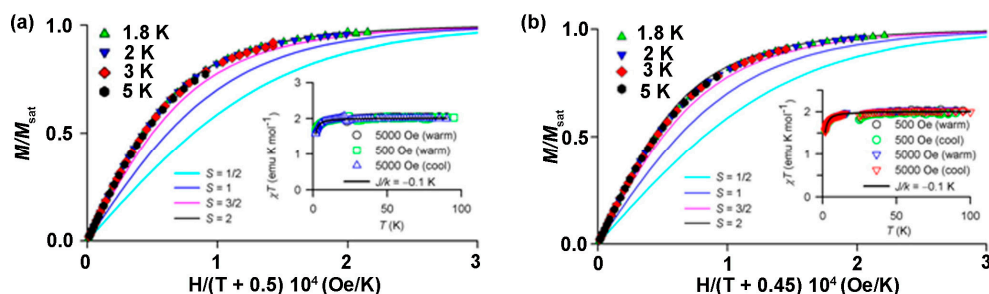


**Figure 14.** A plot of  $M/M_{\text{sat}}$  vs.  $H/(T - \theta)$  from the SQUID magnetometry data of: (a) **128** (6.6 mM) and (b) **129** (7.9 mM) in 2-MeTHF. The magnetization at 1.8, 2, 3, and 5 K is plotted with Brillouin functions for  $S = 1/2, 1, 3/2$ , and 2. Inset plots exhibit the magnetic susceptibility at 500 and 5000 Oe plotted as  $\chi T$  versus  $T$ , and the solid line represents the numerical fit to the Heisenberg Hamiltonian for the dimer of  $S = 2$  tetraradicals. Reproduced from Reference [153]. Copyright 2013, American Chemical Society.

The SQUID magnetometry studies of **128** and **129** in 2-MeTHF verified their quintet ground states, as demonstrated by the  $M$  versus  $H$  and the  $\chi$  versus  $T$  plots. The  $M/M_{\text{sat}}$  versus  $H/(T - \theta)$  plots for **128** and **129** at 1.8–5 K followed the  $S = 2$  Brillouin function. The curvatures of the plots were independent of the radical concentration, which indicated that the measured  $S \approx 2$  is the ground state. Weak intermolecular AFM interactions between the tetraradicals and intra-dimer AFM exchange coupling were implied from the mean field parameter, with  $\theta \approx -0.5$  K.

## 7. H-Bonded TTF-Based Radicals

Mori et al. reported an exceptional H-bond dynamics–based switching of electrical conductivity and magnetism in a deuterated congener, i.e.,  $\kappa$ -D<sub>3</sub> catechol-fused ethylenedithiotetrathiafulvalene (Cat-EDTTTF)<sub>2</sub> (**132**) of an H-bonded organic conductor (Figure 15a) [154]. They found  $\kappa$ -H and  $\kappa$ -D to be isostructural paramagnetic semiconductors having a dimer-Mott-type electronic structure at room temperature. Notably, only  $\kappa$ -D underwent a phase transition at 185 K, and it transforms to a nonmagnetic insulator with a charge-ordered electronic structure.

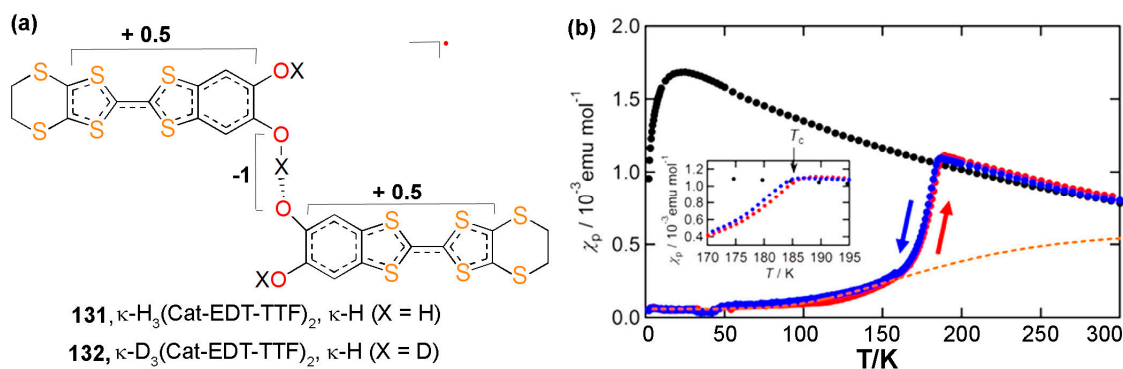


**Figure 15.** (a) Molecule **131** and **132**; (b) Magnetic susceptibility data of  $\kappa$ -D. Cooling and heating processes are represented by blue and red circles, respectively. Black circles represent the cooling process for  $\kappa$ -H. The fitting curve for  $\kappa$ -D by the singlet-triplet dimer model with an AFM coupling of  $2J/k_B \approx -600$  K is represented by the orange line. Reproduced from Reference [154]. Copyright 2014, American Chemical Society.

X-ray crystallographic analysis illustrated that the remarkable switching of the electro-physical properties initiate from D transfer or displacement within the  $[\text{O}\cdots\text{D}\cdots\text{O}]^{-1}$  H-bond. This process was shown to be further complemented by electron transfer between the H-bonded Cat-EDT-TTF  $\pi$ -systems. This corroborated because the H-bonded D dynamics and the conducting TTF  $\pi$ -electron are synergistically coupled. In a pioneering experiment, single crystals of  $\kappa$ -D were prepared from H<sub>2</sub>Cat-EDT-TTF applying a constant current to the H-donor through a simultaneous process of H/D exchange, hydroxyl group exchange, oxidation of the TTFs, and H-bond formation. Importantly, the  $\kappa$ -D crystals were quantitatively deuterated and could be stored under moisture-free conditions for a long time. However, the deuteration ratio was found to be gradually lowered in a few weeks under ambient conditions, possibly as a result of the D/H exchange by atmospheric H<sub>2</sub>O.

They found that the low-temperature (LT) crystal structures of  $\kappa$ -D and  $\kappa$ -H were significantly different from each other. It was in the LT phase ( $\sim 180$  K) that the magnetic susceptibility (Figure 15b) and  $T_C$  were observed, suggesting that the phase transition occurred in association with this crystal structure change. The crystal structure of the LT phase of  $\kappa$ -D at 50 K is shown in Figure 16.

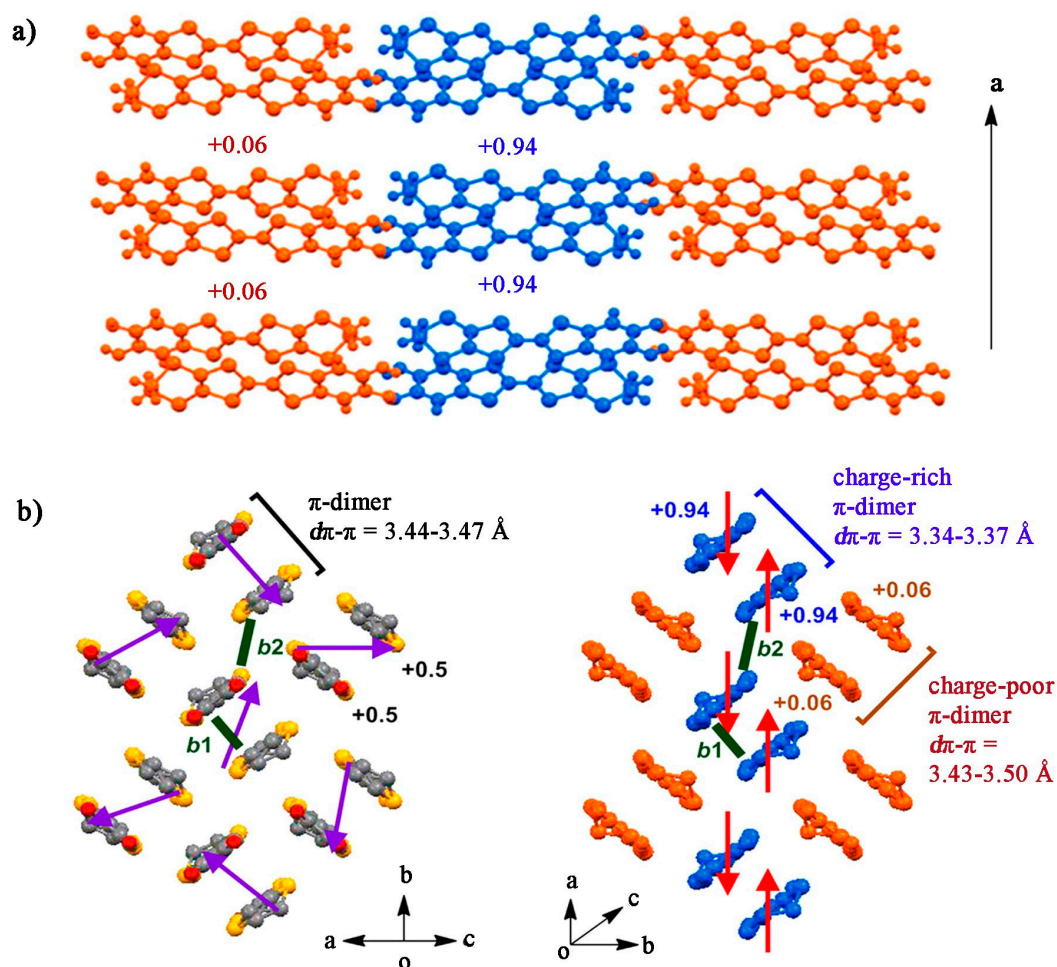


**Figure 16.** A view of the crystal packing of  $\kappa$ -D (132). (a) Arrangement of the Cat-EDT-TTF building blocks at 50 K and (b) within the conducting layer (left: 270 K, right: 50 K). The charge-rich (+0.94) and charge-poor (+0.06) Cat-TTF building blocks, are represented by the blue- and orange-colored molecules, respectively. The intermolecular transfer integrals within and between the  $\pi$ -dimer(s) are represented by parameters  $b_1$  and  $b_2$ , respectively ( $b_1 = 218$  meV,  $b_2 = 79$  meV at 270 K (left) and  $b_1 = 335$  meV,  $b_2 = 79$  meV at 50 K (right)). Reproduced from Reference [154]. Copyright 2014, American Chemical Society.

## 8. Polycyclic Aromatic Hydrocarbon Radicals

The polycyclic aromatic hydrocarbons (PAHs) with an open-shell configuration denote a unique type of hydrocarbon radical comprised of one or more  $\pi$ -electrons which are not firmly paired into the bonding molecular orbital in the ground state. The class of PAHs with two weakly bound  $\pi$ -electrons is referred to as biradicals. The two unpaired electrons can be either in a low-spin singlet or in a high-spin triplet state. A thermally excited transition from the singlet to triplet state can result in a paramagnetic property, although the molecule is a singlet in the ground state. This is only possible if the singlet-triplet energy gap ( $\Delta E_{S-T}$ ) is adequately small. Several types of stable open-shell PAHs have been synthesized: (1) quinodimethane derivatives; (2) phenalenyls; (3) teranthene; and (4) zethrenes. Molecules sustaining a characteristic resonance structure between closed shell and open shell, known as Chichibabin's hydrocarbon, have also been studied in detail.

Wu et al reported derivatives of Chichibabin's hydrocarbon, **133-CS/133-OS** and **134-CS/134-OS** (Figure 17) [155]. The time-dependent UV-vis-NIR absorption spectra of the **133-OS** biradical showed that the absorption spectrum of the biradical diminished with time and the final spectrum after the decay entirely matched with the stable quinoidal form **133-CS** (Figure 18a). Further,  $^1\text{H NMR}$

spectroscopy also nicely delineated this slow relaxation process and established a transition from an unstable **133-OS** to a stable **133-CS**. On the other hand, **134-OS** exhibited a significantly red-shifted absorption in the near-infrared (NIR) region, which was attributed to a small highest occupied molecule orbital and lowest un-occupied molecular orbital HOMO-LUMO energy gap of 1.28 eV (Figure 18b). Notably, even after cooling to  $-100\text{ }^{\circ}\text{C}$ , **134-OS** did not show any NMR signals at room temperature, suggesting the presence of considerable paramagnetic species.

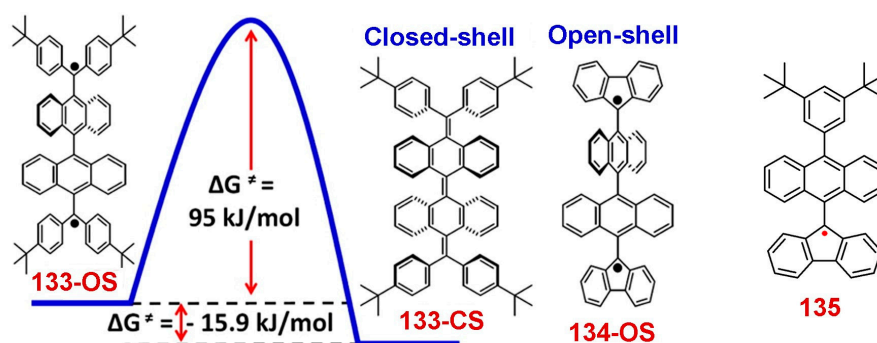


**Figure 17.** Molecular structures of **133-OS/133-CS**, **134-OS** and **135**. Reproduced from Reference [155]. Copyright 2012, American Chemical Society.

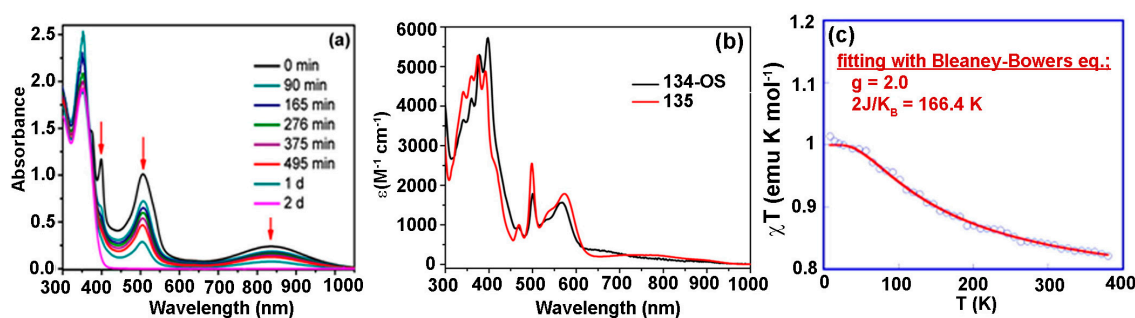


**Figure 18.** (a) UV-vis absorption spectra of the freshly generated **133-OS** biradical and its time-dependent changes; (b) UV-vis-NIR absorption spectrum of **134-OS** and compound **135** in DCM; (c) A plot of  $\chi T$  versus  $T$  of **134-OS** in the SQUID measurements and fitting via the Bleaney-Bowers equation. Reproduced from Reference [155]. Copyright 2012, American Chemical Society.

Next, the SQUID magnetometry studies were performed for **134-OS** in powder form at 5–380 K (Figure 18c). The plot of  $\chi T$  versus temperature and the magnetic susceptibility could be nicely fitted with the Bleaney-Bowers equation. Notably, the singlet-triplet gap was found to be  $2J/k_B = 166\text{ K}$  (1.4 kJ/mol), which suggested that the ground state for **134-OS** is a triplet. Importantly, **2-OS** both in solution and solid states displayed very high stability under ambient air and light conditions for months. The origin of this extraordinary stabilization was ascribed to the fluorenyl and the anthracene units, accounting for the thermodynamic and kinetic stabilization, respectively.

### 8.1. Zethrenes

Zethrenes with six, seven and eight rings (**136**, **137**, and **138**) have been synthesized and studied for their dynamic open-shell to close-shell properties (Chart 9) [156,157]. Recently, Wu et al. reported a series of derivatives of zethrenes: zethrenebis(dicarboximide) (**139**), and heptazethrenebis(dicarboximide) (**140**) [156]. Compound **139** was found to be a closed-shell Kekule hydrocarbon as it exhibited sharp  $^1\text{H-NMR}$  signals at room temperature due to a large singlet-triplet energy gap and only a minute quantity of triplet species. In contrast, **140** revealed a biradical character as the solution in deuterated DCM showed no NMR signals for the heptazethrene core in the aromatic

region. On the other hand, sharp peaks for the heptazethrene backbone started to emerge upon cooling at  $-40$  °C. The absorption spectrum of **140** in chloroform exhibited absorption bands from the far-red to the NIR region with maxima at 827, 747, 701, and 641 nm, further confirming its biradical character (Figure 19a).

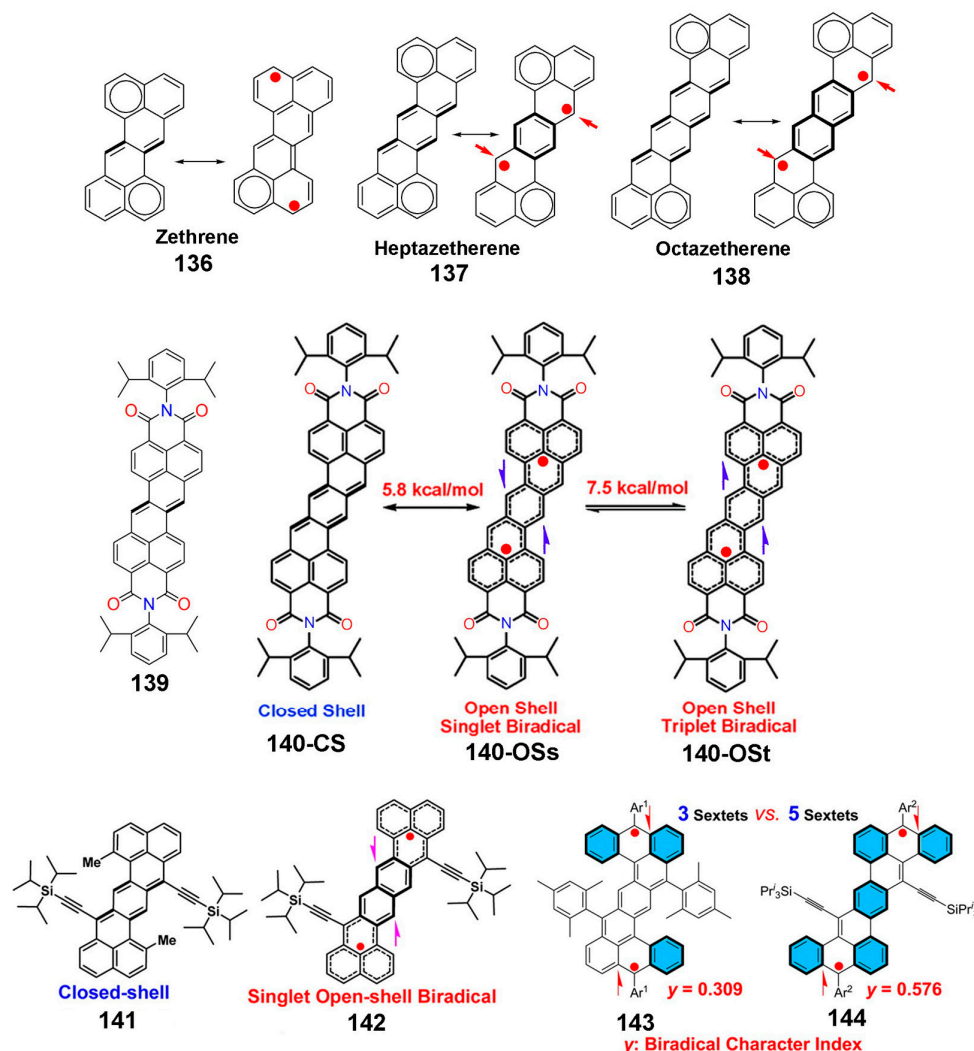
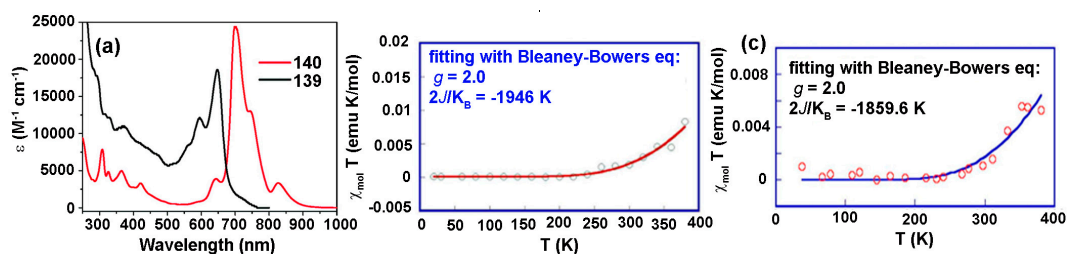
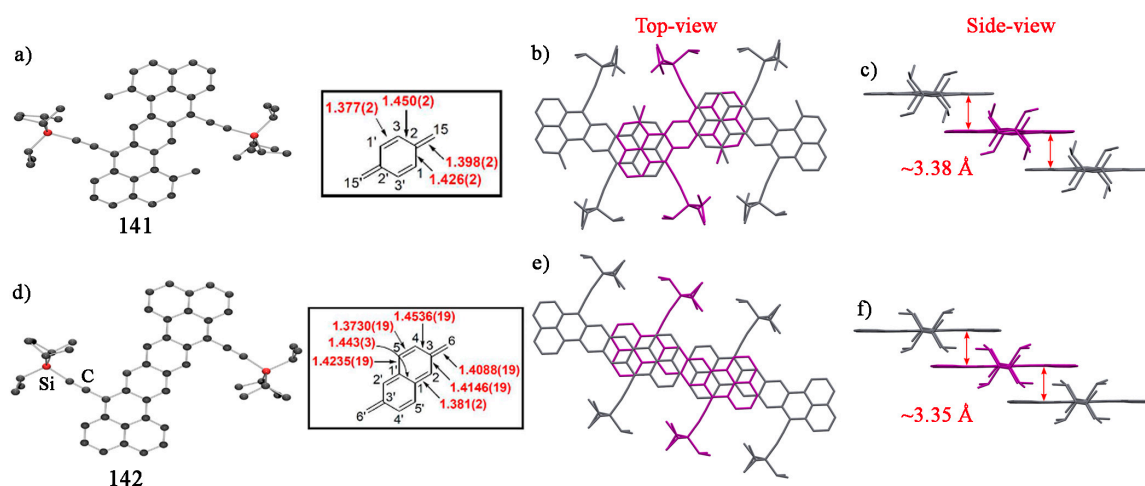


Chart 9. Molecular structures of the zethrene molecules.



**Figure 19.** (a) Absorption spectra of **139** and **140** in chloroform; (b) Plot of  $\chi T$  versus  $T$  for the solid **142**. Open circles represent the measured data. Fitting curve was drawn using the Bleaney-Bowers equation with  $g = 2.00$ ; (c) Plot of  $\chi T$  versus  $T$  for the solid **144**. The measured data were plotted as open circles, and the fitting curve was obtained using the Bleaney-Bowers equation with  $g = 2.00$ . Reproduced from Reference [156–158]. Copyright 2011, 2012, 2013, American Chemical Society.

Wu et al., in a significant modification in their molecular design, reported the kinetically blocked heptazethrene derivative (**141**) and octazethrene derivative (**142**) [157]. Compound **141** was found to have a singlet open-shell ground state and was corroborated by various spectroscopic techniques and also by SQUID measurements. Variable-temperature  $^1\text{H-NMR}$  spectra of **141** in  $\text{CDCl}_3$  were significantly broadened at room temperature and higher temperatures, while the peaks sharpened as the temperature was decreased to  $0\text{ }^\circ\text{C}$ . ESR spectroscopy exhibited a signal at  $g = 2.0026$ . The significantly longer exo-methylene double bonds [ $1.398(2)\text{ \AA}$ ] in **141** and [ $1.4088(19)\text{ \AA}$ ] in **142** compared to those in olefins ( $1.33\text{--}1.34\text{ \AA}$ ) indicated a significant impact of the biradical character (Figure 20). Furthermore, the small but markedly longer exo-methylene bond in **142** suggested a different singlet biradical character.



**Figure 20.** X-ray crystal structure of **141** (a) POV-Ray diagram; (b) top-view and (c) side-view, and **142** (d) POV-Ray diagram; (e) top-view and (f) side-view. Hydrogen atoms have been removed for clarity. Reproduced from Reference [157]. Copyright 2012, American Chemical Society.

The singlet-triplet energy gap ( $\Delta E_{S-T}$ ) of **142** was determined by SQUID measurements at  $5\text{--}380\text{ K}$ . The magnetic measurements revealed an increasing susceptibility above  $220\text{ K}$  (Figure 19b), and a value of  $2J/k_B = -1946\text{ K}$  ( $3.87\text{ kcal/mol}$ ) was obtained by fitting the data using the Bleaney-Bowers equation. A small singlet-triplet energy gap ( $\Delta E_{S-T} \approx 3.87\text{ kcal/mol}$ ) demonstrated that the singlet open-shell ground state of **142** can be thermally excited to its triplet excited state at room temperature. The percentage of the triplet species at room temperature was assessed to be  $\sim 0.14\%$ .

Wu et al. have subsequently reported the two stable dibenzoheptazethrene derivatives **143** and **144** (Chart 9) and their biradical characters [158]. The biradical characters were examined by X-ray crystallographic analysis, spectroscopic measurements, and theoretical studies. The studies afforded the understanding of how Clar's aromatic sextet rule can be applied to the singlet biradicaloids. A distinct ESR signal, the absence of an NMR signal at room temperature and the temperature-dependent magnetic susceptibility behavior of **144** within the range  $5\text{--}380\text{ K}$  established a singlet biradical ground state. The fitting of the data using the Bleaney-Bowers equation revealed an exchange interaction energy ( $2J/k_B$ , i.e.,  $\Delta E_{SB-TB}$ ) of  $-1859.6\text{ K}$  ( $-3.7\text{ kcal/mol}$ ) (Figure 19c).

### 8.2. *P*-Quinodimethane (*p*-QDM)

*p*-QDM is known to have a large biradical character in the ground state as a result of the retrieval of the aromaticity of the benzenoid rings, which also makes them reactive. There have been focused attempts to design and synthesize stable *p*-QDM derivatives and its extended congeners. Wu et

al. have reported a diverse range of stable oligo(N-annulated perylene)quinodimethanes **nPer-CN** ( $n = 1-6$ ) (**145-150**), respectively, comprising up to 12 para-linked benzenoid rings (Figure 21a) [159].

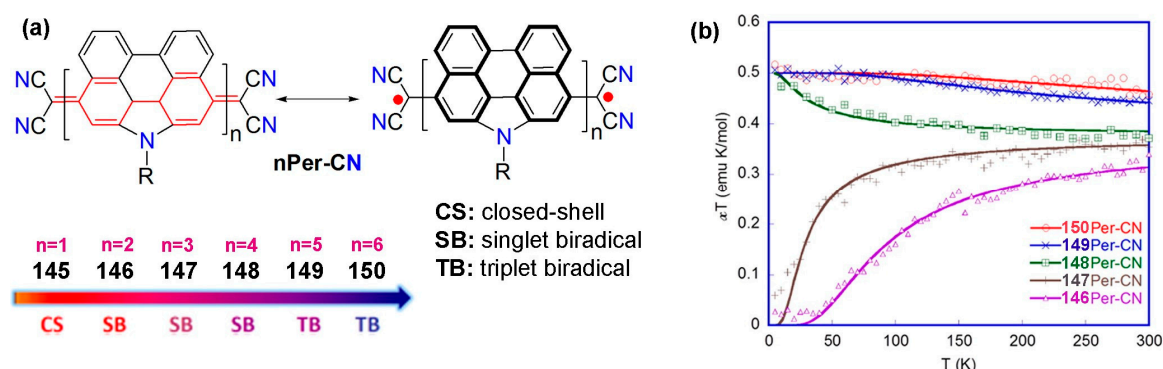


**Figure 21.** (a) Molecular structures of **145-150** and (b) plot of  $\chi T$  versus  $T$  curves of **nPer-CN** ( $n = 2-6$ ) (**146-150**). The solid lines represent the fitting curves obtained from the Bleaney-Bowers equation;  $g = 2.00$ . Reproduced from Reference [159]. Copyright 2013, American Chemical Society.

The smallest derivative, **145**, exhibited well-resolved  $^1\text{H}$  and  $^{13}\text{C}$ -NMR signals in  $\text{CDCl}_3$  at 298 K, suggesting that **145** has a closed-shell quinoidal structure in the ground state. On the other hand, the extended derivatives **146-150** were found to be NMR-silent even at low temperature ( $-100^\circ\text{C}$  in  $\text{CD}_2\text{Cl}_2$ ), suggesting that the extended derivatives have a significant biradical character in the ground state. Derivatives **146-150** exhibited broad ESR signals in the solid as well as solution state with  $g = 2.0031$ .

From the SQUID measurements of **146** and **147** in the powder form at 5–300 K, the singlet-triplet energy gap  $\Delta E_{S-T}$  (i.e.,  $-2J/k_B$ ) was found to be 0.342 and 0.107 kcal/mol for **146** and **147**, respectively (Figure 21b). This further confirmed that both **146** and **147** have a singlet biradical ground state. A very weak coupling between the two radicals could be judged from the small  $\Delta E_{S-T}$  ( $-0.064$  kcal/mol) for **148**. Due to the inevitable error during the data fitting for this borderline molecule, the ground state of **148** was described as a singlet biradical with a very large biradical character based on the variable-temperature ESR experiments and computational studies. Further moving to **149** and **150**, the  $\Delta E_{S-T}$  became  $-0.56$  and  $-0.88$  kcal/mol, respectively, signifying a triplet biradical ground state.

### 8.3. Tetraradicaloids

Wu et al. further reported a series of tetraradicaloid molecules (**151-162**) (Chart 10) [160]. The SQUID measurement of **159** showed that  $\chi T$  increased as the temperature was increased beyond 100 K, which implied a singlet ground state. The  $\Delta E_{S-T}$  was calculated to be  $-852.6$  K ( $-1.69$  kcal/mol) for **159** by fitting of the data using the Bleaney-Bowers equation.

In a very recent report, Wu et al. described the first synthesis of a relatively stable nonazethrene derivative, **163** (Figure 22a) [161]. They found that **163** has an open-shell ground state since the broad  $^1\text{H}$ -NMR spectrum at room temperature got progressively sharpened by lowering the temperature. The ESR signal was found to be strong and broad with a  $g$  value of 2.0027 for both the solid and solution states, confirming its delocalized singlet diradicaloid nature.

SQUID measurements of **163** in the temperature range of 2–380 K showed that  $\chi T$  increased with the increase of the temperature after 250 K (Figure 22b), which correlates to a thermal population from a singlet to a paramagnetic triplet state. The singlet-triplet energy gap ( $\Delta E_{S-T}$ ) was estimated to be  $-5.2$  kcal/mol by fitting the data using the Bleaney-Bowers equation, which was close to the calculated value of  $-5.4$  kcal/mol.

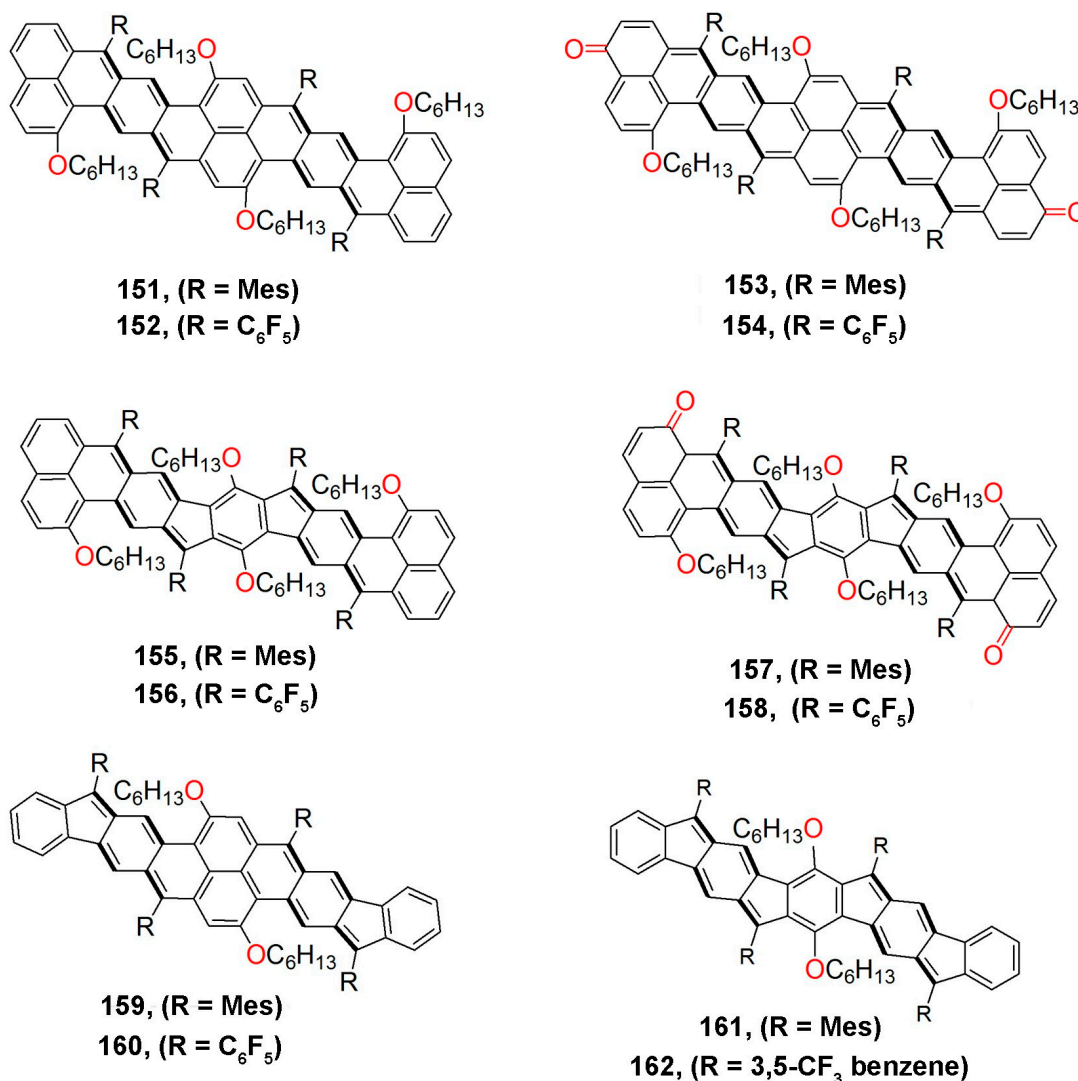
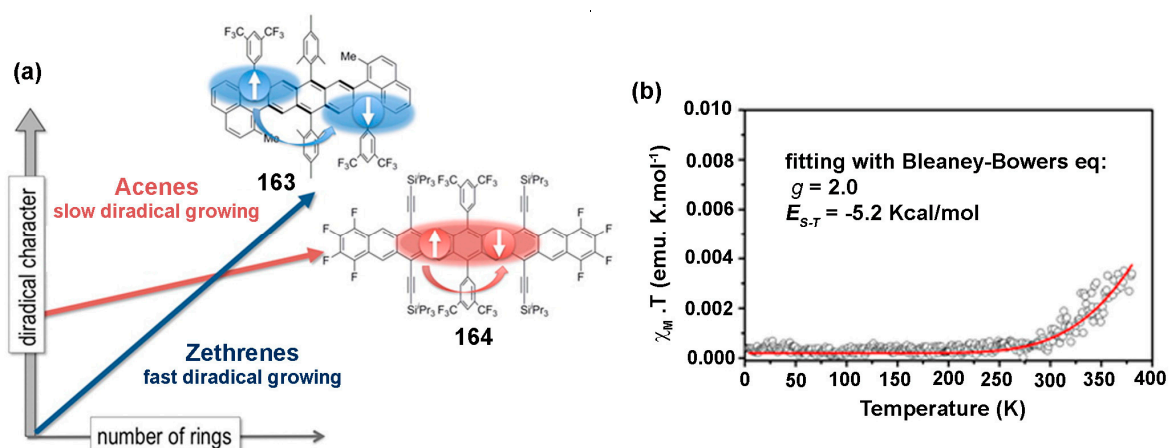


Chart 10. Molecular structures of tetradiracaloid molecules.



**Figure 22.** (a) Molecular structures of **163** and **164**; (b) Plot of  $\chi T$  versus  $T$  plot for the solid sample of **163** in SQUID magnetometry studies. Open circles represent the measured data and the red curve denotes the best fit using the Bleaney-Bowers equation with  $g_e = 2.00$ . Reproduced from Reference [161]. Copyright 2016, American Chemical Society.

## 8.4. Macrocyclic Polyradicals

In a highly innovative design, Wu et al. reported two carbazole-based macrocycles, **165** and **166**, constituting four and six alternately arranged quinoidal and aromatic carbazole units, respectively (Figure 23) [162]. The quinoidal carbazole moiety has a strong propensity to recuperate two aromatic sextet rings in the diradical form, as it can be considered to be an analogue of a pro-aromatic Tschitschibabin's hydrocarbon. Therefore, in **165** and **166**, two aromatic sextets can be accomplished at each transition from the closed-shell to the open-shell diradical form, to the tetraradical form, and ultimately to the hexaradical form.

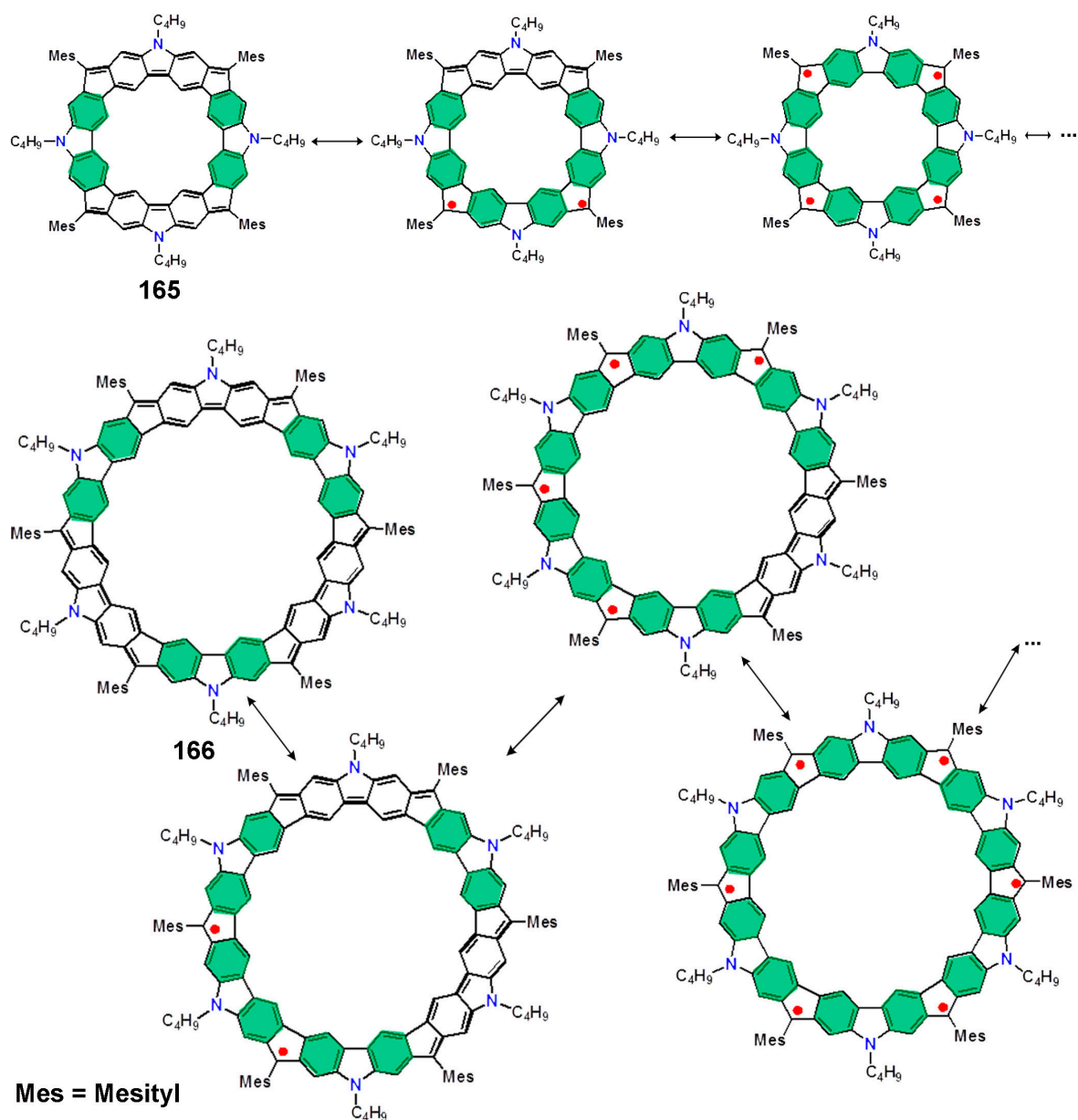


**Figure 23.** Molecular structures of the closed-shell and open-shell canonical forms of **165** and **166**. Mes = mesityl groups. Clar's aromatic sextets are depicted in blue hexagons. Reproduced from Reference [162]. Copyright 2016, American Chemical Society.

The magnetic properties of **165** and **166** in the powder sample were studied in the temperature range of 2–380 K, where **166** showed an increase in the  $\chi T$  above 35 K, which suggested a singlet

ground state. In addition, another clear increase of  $\chi T$  around 250 K was observed, which is possibly related with excitation into other spin states or a phase transition.

The magnetization measurements for **166** established a weak magnetization originating around 200 K, reaching a maximum at 250 K, and then decreasing with the increasing temperature and finally becoming weak at 380 K (Figure 24a,b). This behavior resembles a long-range ordered FM coupling. However, the narrow hysteresis loop suggests that the magnetization should be described as super-paramagnetism. In contrast, **165** showed an increase in magnetic susceptibility above 4 K and relatively weaker magnetization at 300 K (Figure 24c,d). The singlet-triplet energy gap ( $\Delta E_{S-T}$ , i.e.,  $2J/k_B$ ) was found to be  $-0.30$  kcal/mol for **166** and  $-0.25$  kcal/mol for **165**.

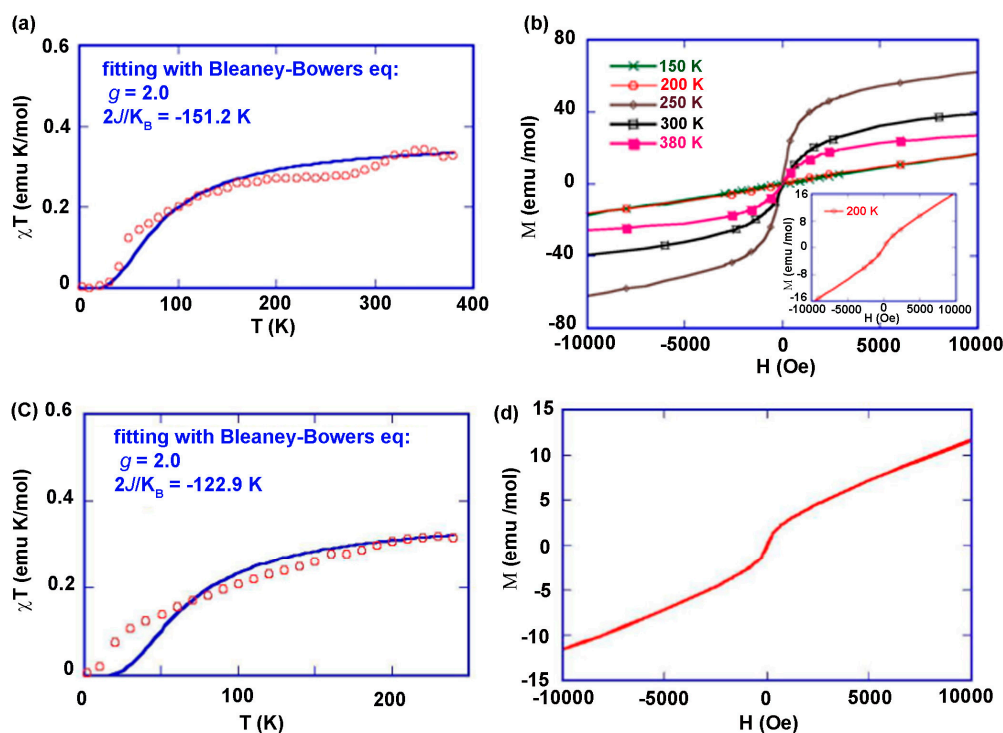


**Figure 24.** (a) The  $\chi T$ - $T$  plot for powder **166**. The measured data were plotted as open circles, and the fitting curve was drawn using the Bleaney-Bowers equation with  $g_e = 2.00$ ; (b) Magnetization curves at different temperatures for the powder of **166**; (c)  $\chi T$ - $T$  plot at different temperatures for the powder of **165**. The measured data were plotted as open circles, and the fitting curve was drawn using the Bleaney-Bowers equation with  $g_e = 2.00$ ; (d) Magnetization curve at 300 K for the powder of **165**. Reproduced from Reference [162]. Copyright 2016, American Chemical Society.

## 9. Conclusions

In summary, we have reviewed the recent advances made in the design and magnetic studies of organic radicals and polyradicals. The  $\pi$ -conjugated organic radicals such as phenalenyl systems, nitronylnitroxides, benzotriazinyl, bithiazolyl and aminyl-based radicals and polyradicals have been considered. The examples clearly show that weak noncovalent interactions play a major role in modulating ferromagnetic and antiferromagnetic properties. We have also deliberated on the emerging direction of zethrenes, organic polyradicals and macrocyclic polyradicals. The review also presents a collation of the major organic neutral radicals, radical ions and radical zwitterions that have emerged over the period of last century.

The organic radicals and radical ions have tremendous future potential in multiple fields pertaining to purely academics as well as applications and technology in the areas of energy storage [163,164], spintronics [16], quantum information processing [165] and sensing [166–168]. For example, the realization of a flexible radical battery from organic radicals is a major step forward

towards the storage of solar or other renewable sources of energy. Electron and nuclear spins as quantum bits (qubits) have been a focus to gain insight and contribute in the areas of quantum information science and technology. Furthermore, the attractive optical characteristics of organic radicals with multi-channel absorption bands in the UV–vis–NIR region, their conductivity and their paramagnetism provide a unique opportunity to probe and detect toxic chemicals in an effective way in comparison to the traditional ways of chemical sensing.

**Acknowledgments:** We thank DST-FIST for funding the instrumentation facilities and DST PURSE, DBT-BUILDER, and UPE-II projects for financial assistance. P.M. thanks DST Govt. of India for the SwarnaJayanti Fellowship (DST/SJF-02/CSA-02/2013-14).

**Author Contributions:** S.K., Y.K., S.K.K. and P.M. wrote the review.

**Conflicts of Interest:** The authors declare no conflict of interest.

## References

1. Iwamura, H. What role has organic chemistry played in the development of molecule-based magnets? *Polyhedron* **2013**, *66*, 3–14. [[CrossRef](#)]
2. Gomberg, M. An instance of trivalent carbon: Triphenylmethyl. *J. Am. Chem. Soc.* **1900**, *22*, 757–771. [[CrossRef](#)]
3. Hicks, R.G. (Ed.) *Stable Radicals: Fundamentals and Applied Aspects of Odd-Electron Compounds*; John Wiley & Sons Ltd.: Chichester, UK, 2010.
4. Abe, M. Diradicals. *Chem. Rev.* **2013**, *113*, 7011–7088. [[CrossRef](#)] [[PubMed](#)]
5. International Union of Pure and Applied Chemistry. *IUPAC Compendium of Chemical Terminology, Release 2.3.2*; International Union of Pure and Applied Chemistry (IUPAC): Research Triangle Park, NC, USA, 2012; p. 168.
6. International Union of Pure and Applied Chemistry. *IUPAC Compendium of Chemical Terminology, Release 2.3.2*; International Union of Pure and Applied Chemistry (IUPAC): Research Triangle Park, NC, USA, 2012; p. 427.
7. Amorati, R.; Lucarini, M.; Mugnaini, V.; Pedulli, G.F.; Minisci, F.; Recupero, F.; Fontana, F.; Astolfi, P.; Greci, L. Hydroxylamines as Oxidation Catalysts: Thermochemical and Kinetic Studies. *J. Org. Chem.* **2003**, *68*, 1747–1754. [[CrossRef](#)] [[PubMed](#)]
8. Zhang, N.; Samanta, S.R.; Rosen, B.M.; Percec, V. Single Electron Transfer in Radical Ion and Radical-Mediated Organic, Materials and Polymer Synthesis. *Chem. Rev.* **2014**, *114*, 5848–5958. [[CrossRef](#)] [[PubMed](#)]
9. Asandei, A.D.; Moran, I.W.; Saha, G.; Chen, Y. Ti-Catalyzed Living radical polymerization of Styrene Initiated by Epoxide radical ring Opening. *ACS Symp. Ser.* **2006**, *944*, 125–139.
10. Asandei, A.D.; Chen, Y. Cp<sub>2</sub>TiCl-Catalyzed SET Reduction of Aldehydes: A New Initiating Protocol for Living Radical Polymerization. *Macromolecules* **2006**, *39*, 7549–7554. [[CrossRef](#)]
11. Suga, T.; Sakata, M.; Aoki, K.; Nishide, H. Synthesis of Pendant Radical- and Ion-Containing Block Copolymers via Ring-Opening Metathesis Polymerization for Organic Resistive Memory. *ACS Macro Lett.* **2014**, *3*, 703–707. [[CrossRef](#)]
12. Gatteschi, D. Molecular Magnetism: A basis for new materials. *Adv. Mater.* **1994**, *6*, 635–645. [[CrossRef](#)]
13. Fujita, W.; Awaga, K. Room-Temperature Magnetic Bistability in Organic Radical Crystals. *Science* **1999**, *286*, 261–262. [[CrossRef](#)] [[PubMed](#)]
14. Janoschka, T.; Hager, M.D.; Schubert, U.S. Powering up the Future: Radical Polymers for Battery Applications. *Adv. Mater.* **2012**, *24*, 6397–6409. [[CrossRef](#)] [[PubMed](#)]
15. Suga, T.; Ohshiro, H.; Sugita, S.; Oyaizu, K.; Nishide, H. Emerging N-Type Redox-Active Radical Polymer for a Totally Organic Polymer-Based Rechargeable Battery. *Adv. Mater.* **2009**, *21*, 1627–1630. [[CrossRef](#)]
16. Gaudenzi, R.; Burzurí, E.; Reta, D.; Moreira, I.P.R.; Bromley, S.T.; Rovira, C.; Veciana, J.; van der Zant, H.S.J. Exchange Coupling Inversion in a High-Spin Organic Triradical Molecule. *Nano Lett.* **2016**, *16*, 2066–2071. [[CrossRef](#)] [[PubMed](#)]
17. Frisenda, R.; Gaudenzi, R.; Franco, C.; Mas-Torrent, M.; Rovira, C.; Veciana, J.; Alcon, I.; Bromley, S.T.; Burzurí, E.; van der Zant, H.S.J. Kondo Effect in a Neutral and Stable All Organic Radical Single Molecule Break Junction. *Nano Lett.* **2015**, *15*, 3109–3114. [[CrossRef](#)] [[PubMed](#)]
18. Hubbell, W.L.; Gross, A.; Langen, R.; Lietzow, M.A. Recent advances in site-directed spin labeling of proteins. *Curr. Opin. Struct. Biol.* **1998**, *8*, 649–656. [[CrossRef](#)]

19. Fanucci, G.E.; Cafiso, D.S. Recent advances and applications of site-directed spin labeling. *Curr. Opin. Struct. Biol.* **2006**, *16*, 644–653. [[CrossRef](#)] [[PubMed](#)]
20. Cambi, L.; Szego, L. Über die magnetische Suszeptibilität der komplexen Verbindungen. *Ber. Dtsch. Chem. Ges. B* **1931**, *64*, 2591–2598. [[CrossRef](#)]
21. Ratera, I.; Veciana, J. Playing with organic radicals as building blocks for functional molecular materials. *Chem. Soc. Rev.* **2012**, *41*, 303–349. [[CrossRef](#)] [[PubMed](#)]
22. Fourmigué, M.; Liefbrig, J. Organizing Radical Species in the Solid State with Halogen Bonding. *Top. Curr. Chem.* **2015**, *359*, 91–114. [[PubMed](#)]
23. Tamura, M.; Nakazawa, Y.; Shiomi, D.; Nozawa, K.; Hosokoshi, Y.; Ishikawa, M.; Takahashi, M.; Kinoshita, M. Bulk ferromagnetism in the  $\beta$ -phase crystal of the p-nitrophenyl nitronyl nitroxide radical. *Chem. Phys. Lett.* **1991**, *186*, 401–404. [[CrossRef](#)]
24. Banister, A.J.; Bricklebank, N.; Lavender, I.; Rawson, J.M.; Gregory, C.I.; Tanner, B.K.; Clegg, W.; Elsegood, M.R.J.; Palacio, F. Spontaneous magnetization in a sulfur-nitrogen radical at 36 K. *Angew. Chemie Int. Ed.* **1996**, *35*, 2533–2535. [[CrossRef](#)]
25. Piloty, O.; Schwerin, B.G. Ueber die Existenz von Derivaten des vierwertigen Stickstoffs (I. Mittheilung). *Chem. Ber.* **1901**, *34*, 1870–1887. [[CrossRef](#)]
26. Thiele, J.; Balhorn, H. Ueber einen chinoïden Kohlenwasserstoff. *Chem. Ber.* **1904**, *37*, 1463–1470. [[CrossRef](#)]
27. Montgomery, L.K.; Huffman, J.C.; Jurczak, E.A.; Grendze, M.P. The molecular structures of Thiele's and Chichibabin's hydrocarbons. *J. Am. Chem. Soc.* **1986**, *108*, 6004–6011. [[CrossRef](#)] [[PubMed](#)]
28. Tschitschibabin, A.E. Über einige phenylierte Derivate des *p*, *p*-Ditolyls. *Chem. Ber.* **1907**, *40*, 1810–1819. [[CrossRef](#)]
29. Goldschmidt, S.; Renn, K. Zweiwertiger stickstoff: Über das  $\alpha,\alpha$ -diphenyl- $\beta$ -trinitrophenyl hydrazyl. *Ber. Dtsch. Chem. Ges. B* **1922**, *B55*, 628–643. [[CrossRef](#)]
30. Foti, M.C. Use and Abuse of the DPPH• Radical. *J. Agric. Food Chem.* **2015**, *63*, 8765–8876. [[CrossRef](#)] [[PubMed](#)]
31. Reid, D.H. Syntheses and properties of the perinaphthyl radical. *Chem. Ind.* **1956**, 1504–1505.
32. Paskovichlb, D.H.; Reddoch, A.H. Phenalenyl dimer cation and its electron paramagnetic resonance spectrum. *J. Am. Chem. Soc.* **1972**, *94*, 6938–6939. [[CrossRef](#)]
33. Coppinger, G.M. A Stable Phenoxy Radical Inert to Oxygen. *J. Am. Chem. Soc.* **1957**, *79*, 501–502. [[CrossRef](#)]
34. Lebedev, O.L.; Kazarnovskii, S.N. *Zhur. Obshch. Khim.* **1960**, *30*, 1631–1635.
35. Neiman, M.; Rozantzev, É.G.; Mamedova, Y.G. Free radical reactions involving no unpaired electrons. *Nature* **1962**, *196*, 472–473. [[CrossRef](#)]
36. Neiman, M.; Rozantzev, É.G.; Mamedova, Y.G. A new organic radical reaction involving no free valence. *Nature* **1963**, *200*, 256. [[CrossRef](#)]
37. Forrester, A.R.; Thomson, R.H. Stable nitroxide radical. *Nature* **1964**, *203*, 74–75. [[CrossRef](#)]
38. Keana, J.F.W. Newer aspects of the synthesis and chemistry of nitroxide spin labels. *Chem. Rev.* **1978**, *78*, 37–64. [[CrossRef](#)]
39. Kuhn, R.; Trischmann, H. Surprisingly Stable Nitrogenous Free Radicals. *Angew. Chem. Int. Ed.* **1963**, *2*, 155. [[CrossRef](#)]
40. Neugebauer, F.A. Hydrazidiny radicals: 1,2,4,5-Tetraazapentenyls, Verdazyls, and Tetrazolinyls. *Angew. Chem. Int. Ed.* **1973**, *12*, 455–464. [[CrossRef](#)]
41. Barr, C.L.; Chase, P.A.; Hicks, R.G.; Lemaire, M.T.; Stevens, C.L. Synthesis and characterization of verdazyl radicals bearing pyridine or pyrimidine substituents: A new family of chelating spin-bearing ligands. *J. Org. Chem.* **1999**, *64*, 8893–8897. [[CrossRef](#)] [[PubMed](#)]
42. Kuhn, R.; Neugebauer, F.A.; Trischmann, H. Tetraazapentenyl radicals. *Angew. Chem. Int. Ed.* **1964**, *3*, 232. [[CrossRef](#)]
43. Kosower, E.M.; Poziomek, E.J. Stable Free Radicals. I. Isolation and Distillation of 1-Ethyl-4-carbomethoxy-pyridinyl. *J. Am. Chem. Soc.* **1964**, *86*, 5515–5523. [[CrossRef](#)]
44. Kuhn, R.; Neugebauer, F.A.; Trischmann, H. Stabile N-haltige Biradikale und Triradikale. *Monatsh. Chem.* **1966**, *97*, 525–553. [[CrossRef](#)]
45. Keana, J.F.W.; Keana, S.B.; Beetham, D. A New Versatile Ketone Spin Label. *J. Am. Chem. Soc.* **1967**, *89*, 3055–3056. [[CrossRef](#)]

46. Osiecki, J.H.; Ullman, E.F. Studies of Free Radicals. I. a-Nitronyl Nitroxides a New Class of Stable Radicals. *J. Am. Chem. Soc.* **1968**, *90*, 1078–1079. [[CrossRef](#)]
47. Blatter, H.M.; Lukaszewski, H. A new stable free radical. *Tetrahedron Lett.* **1968**, *9*, 2701–2705. [[CrossRef](#)]
48. Berezin, A.A.; Constantinides, C.P.; Drouza, C.; Manoli, M.; Koutentis, P.A. From blatter radical to 7-substituted 1,3-diphenyl-1,4-dihydrothiazolo[5',4':4,5]benzo[1,2-e][1,2,4]triazin-4-yls: Toward multifunctional materials. *Org. Lett.* **2012**, *14*, 5586–5589. [[CrossRef](#)] [[PubMed](#)]
49. Neugebauer, F.A. Crystalline tetrazolanyl radical. *Angew. Chem. Int. Ed.* **1969**, *8*, 520–521. [[CrossRef](#)] [[PubMed](#)]
50. Ullman, E.F.; Boocock, D.G.B.J. “Conjugated” nitronyl-nitroxide and imino-nitroxide biradicals. *Chem. Soc. Chem. Commun.* **1969**, 1161–1162. [[CrossRef](#)]
51. Alies, F.; Luneau, D.; Laugier, J.; Rey, P. Ullman’s Nitroxide Biradicals Revisited. Structural and Magnetic Properties. *J. Phys. Chem.* **1993**, *97*, 2922–2925. [[CrossRef](#)]
52. Ballester, M.; Castañer, J.; Olivella, S. Syntheses and isolation of the perchlorodiphenylaminyl, an exceptionally stable radical. *Tetrahedron Lett.* **1974**, *15*, 615–616. [[CrossRef](#)]
53. Yozo, M.; Masayoshi, K. ESR studies of nitrogen-centered free radicals, N-Aryl-N-phenylthioaminyls. *Bull. Chem. Soc. Jpn.* **1977**, *50*, 1142–1146.
54. Markovski, L.N.; Polumbrik, O.M.; Talanov, V.; Shermolovich, Y.G. 1,2,3,5-Dithiadiazolyles, a new type of persistent sulfurnitrogencontaining radicals. *Tetrahedron Lett.* **1982**, *23*, 761–762. [[CrossRef](#)]
55. Barclay, T.M.; Cordes, A.W.; Laat, R.H.; Goddard, J.D.; Haddon, R.C.; Jeter, D.Y.; Mawhinney, R.C.; Oakley, R.T.; Palstra, T.T.M.; Patenaude, G.W.; et al. The heterocyclic diradical benzo-1,2:4,5-bis(1,3,2-dithiazolyl). Electronic, molecular and solid state structure. *J. Am. Chem. Soc.* **1997**, *119*, 2633–2641. [[CrossRef](#)]
56. Mayer, R. S,N-Compounds via Amines and Sulphur Halides. *Phosphorus, Sulfur Silicon Relat. Elem.* **1985**, *23*, 277. [[CrossRef](#)]
57. Preuss, K.E. Metal complexes of thiazyl radicals. *Dalt. Trans.* **2007**, *23*, 2357–2369. [[CrossRef](#)]
58. Haider, K.; Soundararajan, N.; Shaffer, M.; Platz, M.S. EPR spectroscopy of a diaza derivative of meta-xylylene. *Tetrahedron Lett.* **1989**, *30*, 1225–1228. [[CrossRef](#)]
59. Akita, T.; Mazaki, Y.; Kobayashi, K. Crystal Structures and Magnetic Properties of Nitronyl Nitroxide and Imino Nitroxide Radicals Attached to Thieno[3,2-b]-Thieno[2,3-b] thiophene Rings. *J. Org. Chem.* **1995**, *60*, 2092–2098. [[CrossRef](#)]
60. Miura, Y.; Kurokawa, S.; Nakatsuji, M.K.; Teki, Y. Pyridyl-substituted thioaminyl stable free radicals: Isolation, ESR spectra, and magnetic characterization. *J. Org. Chem.* **1998**, *63*, 8295–8303. [[CrossRef](#)]
61. Chi, X.; Itkis, M.E.; Patrik, B.O.; Barklay, T.M.; Reed, R.W.; Oakley, R.T.; Cordes, A.W.; Haddon, R.C. The first phenalenyl-based neutral radical molecular conductor. *J. Am. Chem. Soc.* **1999**, *121*, 10395–10402. [[CrossRef](#)]
62. Mandal, S.K.; Samanta, S.; Itkis, M.E.; Jensen, D.W.; Reed, R.W.; Oakley, R.T.; Tham, F.S.; Donnadiu, B.; Haddon, R.C. Resonating valence bond ground state in oxygen-functionalized phenalenyl-based neutral radical molecular conductors. *J. Am. Chem. Soc.* **2006**, *128*, 1982–1994. [[CrossRef](#)] [[PubMed](#)]
63. Beer, L.; Brusso, J.L.; Cordes, A.W.; Haddon, R.C.; Itkis, M.E.; Kirschbaum, K.; MacGregor, D.S.; Barklay, T.M.; Pinkerton, A.A.; Reed, R.W. Resonance-stabilized 1,2,3-dithiazolo-1,2,3-dithiazolyls as neutral  $\pi$ -radical conductors. *J. Am. Chem. Soc.* **2002**, *124*, 9498–9509. [[CrossRef](#)] [[PubMed](#)]
64. Robertson, C.M.; Leitch, A.A.; Cvrkalj, K.; Myles, D.J.T.; Reed, R.W.; Dube, P.A.; Oakley, R.T. Ferromagnetic ordering in bithiaselenazolyl radicals: Variations on a tetragonal theme. *J. Am. Chem. Soc.* **2008**, *130*, 14791–14801. [[CrossRef](#)] [[PubMed](#)]
65. Sugano, T.; Blundell, S.J.; Hayes, W.; Day, P. Magnetism in organic diradical ion salts based on nitronyl nitroxide. *Polyhedron* **2005**, *24*, 2108–2111. [[CrossRef](#)]
66. Rajca, A.; Shiraishi, K.; Pink, M.; Rajca, S. Triplet ( $S = 1$ ) ground state aminyl diradical. *J. Am. Chem. Soc.* **2007**, *129*, 7232–7233. [[CrossRef](#)] [[PubMed](#)]
67. Rajca, A.; Olankitwanit, A.; Rajca, S. Triplet ground state derivative of aza-m-xylylene diradical with large singlet-triplet energy gap. *J. Am. Chem. Soc.* **2011**, *133*, 4750–4753. [[CrossRef](#)] [[PubMed](#)]
68. Suzuki, S.; Furui, T.; Kuratsu, M.; Kozaki, M.; Shiomi, D.; Sato, K.; Takui, T.; Okada, K. Nitroxide-substituted nitronyl nitroxide and iminonitroxide. *J. Am. Chem. Soc.* **2010**, *132*, 15908–15910. [[CrossRef](#)] [[PubMed](#)]
69. Mahoney, J.K.; Martin, D.; Moore, C.E.; Rheingold, A.L.; Bertrand, G. Bottleable (Amino) (carboxy) Radicals Derived from Cyclic (Alkyl)(Amino) Carbenes. *J. Am. Chem. Soc.* **2013**, *135*, 18766–18769. [[CrossRef](#)] [[PubMed](#)]

70. Bardelang, D.; Casano, G.; Poulhès, F.; Karoui, H.; Filippini, J.; Rockenbauer, A.; Rosas, R.; monnier, V.; Siri, D.; Gaudel-Siri, A.; et al. Spin exchange monitoring of the strong positive homotropic allosteric binding of a tetradical by a synthetic receptor in water. *J. Am. Chem. Soc.* **2014**, *136*, 17570–17577. [[CrossRef](#)] [[PubMed](#)]
71. Gallagher, N.M.; Bauer, J.J.; Pink, M.; Rajca, S.; Rajca, A. High Spin Organic Diradical with Robust Stability. *J. Am. Chem. Soc.* **2016**, *138*, 9377–9380. [[CrossRef](#)] [[PubMed](#)]
72. Bechman, F.; Paul, T. Verhalten von Ketonen und Aldehyden gegen Natrium bei Gegenwart indifferenten Lösungsmittel. *Justus Liebigs Ann. Chem.* **1891**, *266*, 1–28. [[CrossRef](#)]
73. Schlenk, W.; Appenrodt, J.; Michael, A.; Thal, A. Metal additions to multiple bonds. *Ber. Dtsch. Chem. Ges.* **1914**, *47*, 473–490. [[CrossRef](#)]
74. Holy, N.L. Reactions of the radical anions and dianions of aromatic hydrocarbons. *Chem. Rev.* **1974**, *74*, 243–277. [[CrossRef](#)]
75. Scott, N.D.; Walker, J.F.; Hansley, V.L. Sodium Naphthalene. I. A New Method for the Preparation of Addition Compounds of Alkali Metals and Polycyclic Aromatic Hydrocarbons. *J. Am. Chem. Soc.* **1936**, *58*, 2442–2444. [[CrossRef](#)]
76. Acker, S.D.; Hertler, W.R. Substituted Quinodimethans. I. Preparation and Chemistry of 7,7,8,8-Tetracyanoquinodimethan. *J. Am. Chem. Soc.* **1962**, *84*, 3370–3374. [[CrossRef](#)]
77. Eastman, J.W.; Engelsma, G.; Celvin, M. Free Radicals, Ions and Donor-acceptor Complexes in the Reaction: Chloranil + N,N-Dimethylaniline → Crystal Violet. *J. Am. Chem. Soc.* **1962**, *84*, 1339–1345. [[CrossRef](#)]
78. Brandon, R.L.; Osiecki, J.H.; Ottenberg, A. The Reactions of Metallocenes with Electron Acceptors. *J. Org. Chem.* **1966**, *31*, 1214–1217. [[CrossRef](#)]
79. Miller, J.S.; Krusic, P.J.; Dixon, D.A.; Reiff, M.W.; Zhang, J.H.; Anderson, E.C.; Epstein, A.J. Radical Ion Salts of 2,3-Dichloro-5,6-dicyanobenzoquinone and Metallocenes. *J. Am. Chem. Soc.* **1986**, *108*, 4459–4466. [[CrossRef](#)]
80. Walker, D.; Hiebert, J.D. 2,3-Dichloro-5,6-Dicyanobenzoquinone and Its Reactions. *Chem. Rev.* **1967**, *67*, 153–195. [[CrossRef](#)] [[PubMed](#)]
81. Nelsen, S.F. Heterocyclic Radical Anions. 11. Naphthalic and 1,4,5,8-Naphthalenetetracarboxylic Acid Derivatives. *J. Am. Chem. Soc.* **1967**, *190*, 5925–5931. [[CrossRef](#)]
82. Leffler, J.E.; Watts, G.B.; Tanigaki, T.; Dolan, E.; Miller, D.S. Triarylboron anion radicals and the reductive cleavage of boron compounds. *J. Am. Chem. Soc.* **1970**, *92*, 6825–6830. [[CrossRef](#)]
83. Wheland, R.C.; Gillson, J.L. Synthesis of Electrically Conductive Organic. *J. Am. Chem. Soc.* **1976**, *98*, 3916–3925. [[CrossRef](#)]
84. Kaim, W.; Bock, H. Radical Anion and Radical Trianion of 1,4-Bis (dirmethylphosphino) benzene. *J. Am. Chem. Soc.* **1978**, *100*, 6504–6506. [[CrossRef](#)]
85. Rohrbach, W.D.; Gerson, F.; Moeckel, R.; Boekelheide, V. Synthesis of anti-4,5,14,15-tetramethyl[2,2] (2,7)naphthalenophane-1,11-diene and its dianion. ESR and ENDOR studies of its radical anion and other related radical ions. *J. Org. Chem.* **1984**, *49*, 4128–4132. [[CrossRef](#)]
86. Heywang, G.; Born, L.; Fitzky, H.-G.; Hassel, T.; Hocker, J.; Muller, H.-K.; Pittel, B.; Roth, S. Radical Anion Salts of Naphthalenetetracarboxylic Acid Derivatives—a Novel Class of Electrically Conducting Compounds. *Angew. Chem. Int. Ed.* **1989**, *28*, 483–485. [[CrossRef](#)]
87. Zhao, J.; Dowd, P.; Grabowski, J.J. Anion-molecule approaches to non-kekule molecules: The radical anion of cyclopentadienyliidenetrimethylenemethane and derivatives. *J. Am. Chem. Soc.* **1996**, *118*, 8871–8874. [[CrossRef](#)]
88. Schmitt, S.; Baumgarten, M.; Simon, J.; Hafner, K. 2,4,6,8-Tetracyanoazulene: A New Building Block for ‘Organic Metals’. *Angew. Chem. Int. Ed.* **1998**, *37*, 1077–1081. [[CrossRef](#)]
89. Gosztoła, D.; Niemczyk, M.P.; Svec, W.; Lukas, A.S.; Wasielewski, M.R. Excited Doublet States of Electrochemically Generated Aromatic Imide and Diimide Radical Anions. *J. Phys. Chem. A* **2000**, *104*, 6545–6655. [[CrossRef](#)]
90. Ishida, S.; Iwamoto, T.; Kira, M. Radical anion of isolable dialkylsilylene. *J. Am. Chem. Soc.* **2003**, *125*, 3212–3213. [[CrossRef](#)] [[PubMed](#)]
91. Nelsen, S.F.; Weaver, M.N.; Konradsson, A.E.; Telo, J.P.; Clark, T. Electron transfer within 2,7-dinitronaphthalene radical anion. *J. Am. Chem. Soc.* **2004**, *126*, 15431–15438. [[CrossRef](#)] [[PubMed](#)]

92. Makarov, A.Y.; Irtegov, I.G.; Vasilieva, N.V.; Bagryanskaya, I.Y.; Borrmann, T.; Gatilov, Y.V.; Lork, E.; Mews, R.; Stohrer, W.-D.; Zibarev, A.V. [1,2,5]Thiadiazolo[3,4-c][1,2,5]thiadiazolidyl: A Long-Lived Radical Anion and Its Stable Salts. *Inorg. Chem.* **2005**, *44*, 7194–7199. [[CrossRef](#)] [[PubMed](#)]
93. Denning, M.S.; Irwin, M.; Goicoechea, J.M. Synthesis and Characterization of the 4,4'-Bipyridyl Dianion and Radical Monoanion. A Structural Study. *Inorg. Chem.* **2008**, *47*, 6118–6120. [[CrossRef](#)] [[PubMed](#)]
94. Nelsen, S.F.; Weaver, M.N.; Telo, J.P. Solvent Control of Charge Localization in 11-Bond Bridged Dinitroaromatic Radical Anions. *J. Am. Chem. Soc.* **2007**, *129*, 7036–7043. [[CrossRef](#)] [[PubMed](#)]
95. Kozaki, M.; Sugimura, K.; Ohnishi, H.; Okada, K. Preparation, Properties, and Reduction of a Novel TCNQ-Type Thienoquinoid. *Org. Lett.* **2006**, *8*, 5235–5238. [[CrossRef](#)] [[PubMed](#)]
96. Rosokha, S.V.; Lu, J.; Han, B.; Kochi, J.K. Unusual structural effects of intermolecular  $\pi$ -bonding in the tetracyanopyrazine (ion-radical) dimer. *New J. Chem.* **2009**, *33*, 545–553. [[CrossRef](#)]
97. Ueda, A.; Ogasawara, K.; Nishida, S.; Ise, T.; Yoshino, T.; Nakazawa, S.; Sato, K.; Takui, T.; Nakasuji, K.; Morita, Y. A bowl-shaped ortho-semiquinone radical anion: Quantitative evaluation of the dynamic behavior of structural and electronic features. *Angew. Chem. Int. Ed.* **2010**, *49*, 6333–6337. [[CrossRef](#)] [[PubMed](#)]
98. Ajayakumar, M.R.; Asthana, D.; Mukhopadhyay, P. Core-modified naphthalenediimides generate persistent radical anion and cation: New panchromatic NIR probes. *Org. Lett.* **2012**, *14*, 4822–4825. [[CrossRef](#)] [[PubMed](#)]
99. Kushida, T.; Yamaguchi, S. A radical anion of structurally constrained triphenylborane. *Organometallics* **2013**, *32*, 6654–6657. [[CrossRef](#)]
100. Roznyatovskiy, V.V.; Gardner, D.M.; Eaton, S.W.; Wasielewski, M.R. Radical Anions of trifluoromethylated perylene and naphthalene imide and diimide electron acceptors. *Org. Lett.* **2014**, *16*, 696–699. [[CrossRef](#)] [[PubMed](#)]
101. Pan, X.; Weng, X.; Zhao, Y.; Sui, Y.; Wang, X. A crystalline phosphalkene radical anion. *J. Am. Chem. Soc.* **2014**, *136*, 9834–9837. [[CrossRef](#)] [[PubMed](#)]
102. Mizuno, A.; Shuku, Y.; Suizu, R.; Matsushita, M.M.; Tsuchiizu, M.; Mañeru, D.R.; Illas, F.; Robert, V.; Awaga, K. Discovery of the K<sub>4</sub> Structure Formed by a Triangular  $\pi$  Radical Anion. *J. Am. Chem. Soc.* **2015**, *137*, 7612–7615. [[CrossRef](#)] [[PubMed](#)]
103. Peters, S.J.; Klen, J.R. Tris-[8]annulenyl isocyanurate trianion triradical and hexa-anion from the alkali metal reduction of [8]annulenyl isocyanate. *J. Org. Chem.* **2015**, *80*, 5851–5858. [[CrossRef](#)] [[PubMed](#)]
104. Ji, L.; Haehnel, M.; Krummenacher, I.; Biegger, P.; Geyer, F.L.; Tverskoy, O.; Schaffroth, M.; Han, J.; Dreuw, A.; Marder, T.B.; et al. The Radical Anion and Dianion of Tetraazapentacene. *Angew. Chem. Int. Ed.* **2016**, *55*, 10498–10501. [[CrossRef](#)] [[PubMed](#)]
105. Wurster, C.; Sendtner, R. Zur Kenntniss des Dimethylparaphenylendiamins. *Ber. Dtsch. Chem. Ges.* **1879**, *12*, 1803–1807. [[CrossRef](#)]
106. Wurster, C.; Scholig, E. Ueber die Einwirkung oxydirender Agentien auf Tetramethylparaphenylendiamin. *Ber. Dtsch. Chem. Ges.* **1879**, *12*, 1807–1813. [[CrossRef](#)]
107. Wieland, H. Zur Kenntnis der tertiären aromatischen Hydrazine und Amine. (III). *Chem. Ber.* **1907**, *40*, 4260–4281. [[CrossRef](#)]
108. Weitz, E.; Schwechthin, H.W. Über den Ammonium-Charakter der Triarylamine. (VII. Mitteilung über freie Ammonium-Radikale.). *Chem. Ber.* **1926**, *59*, 2307–2314. [[CrossRef](#)]
109. Michaelis, L. "Ein Reduktions-Indikator im Potentialbereich der Wasserstoffüberspannung". *Biochem. Zeitschrift* **1932**, *250*, 564–567.
110. Michaelis, L.; Hill, E.S.J. The Viologen Indicator. *Gen. Physiol.* **1933**, *16*, 859–873. [[CrossRef](#)]
111. Bockman, T.M.; Kochi, J.K. Isolation and Oxidation-Reduction of methylviologen cation radicals. Novel disproportionation in charge-transfersalts by X-ray crystallography. *J. Org. Chem.* **1990**, *55*, 4127–4135. [[CrossRef](#)]
112. Lewis, I.C.; Singer, L.S. Electron spin resonance of radical cations produced by the oxidation of aromatic hydrocarbons with SbCl<sub>5</sub>. *J. Chem. Phys.* **1965**, *43*, 2712–2727. [[CrossRef](#)]
113. McKinney, T.M.; Geske, D.H. The triethylenediamine cation radical. *J. Am. Chem. Soc.* **1965**, *87*, 3013–3014. [[CrossRef](#)]
114. Nelson, R.F.; Adams, R.N. The anion and cation radicals of N,N-dimethyl-p-nitroaniline. *J. Phys. Chem.* **1968**, *72*, 740–742. [[CrossRef](#)]

115. Ishizu, K.; Dearman, H.H.; Huang, M.T.; White, J.R. Interaction of the 5-Methylphenazinium cation radical with deoxyribonucleic acid. *Biochemistry* **1969**, *8*, 1238–1246. [[CrossRef](#)] [[PubMed](#)]
116. Wudl, F.; Wobschall, D.; Hufnagel, E.J. Electrical conductivity by the bis-1,3-dithiole-bis-1,3-dithiolium system. *J. Am. Chem. Soc.* **1972**, *94*, 670–672. [[CrossRef](#)]
117. Drews, M.J.; Wong, P.S.; Jones, P.R. Bonding studies in group IV substituted anilines. III. Electron spin resonance spectra of the radical cations and the ground-state bonding description. *J. Am. Chem. Soc.* **1972**, *94*, 9122–9128. [[CrossRef](#)]
118. Effenberger, F.; Mack, K.E.; Niess, R.; Reisinger, F.; Steinbach, A.; Stohrer, W.D.; Stezowski, J.J.; Rommel, I.; Maier, A. Aminobenzenes. 19' dimeric  $\alpha$ -complexes: Intermediates in the oxidative dimerization of aromatics. *J. Org. Chem.* **1988**, *53*, 4379–4386. [[CrossRef](#)]
119. Effenberger, F.; Stohrer, W.D.; Mack, K.E.; Reisinger, F.; Seufert, W.; Kramer, H.E.A.; Foll, R.; Vogelmann, E. Experimental and theoretical aspects of the formation of radical cations from tripyrrolidinobenzenes and their follow-up reactions. *J. Am. Chem. Soc.* **1990**, *112*, 4849–4857. [[CrossRef](#)]
120. Schmittel, M.; Gescheidt, G.; Rock, M. The first spectroscopic identification of an enol radical cation in solution: The anisylidimesitylethenol radical cation. *Angew. Chem. Int. Ed.* **1994**, *33*, 1961–1963. [[CrossRef](#)]
121. Adam, W.; Kammel, T. Generation of 4,5-diazacyclopentane-1,3-diyl radical cations by chemical electron transfer (CET) oxidation of urazole-bridged bicyclic housanes (Bicyclo[2.1.0]pentanes) and their chemical transformations. *J. Org. Chem.* **1996**, *61*, 3172–3176. [[CrossRef](#)] [[PubMed](#)]
122. Bryce, M.R.; Moore, A.J. Vinylogous tetrathiafulvalene (TTF)  $\alpha$ -electron donors and derived radical cations: ESR spectroscopic, magnetic, and X-ray structural studies. *Chem. Mater.* **1996**, *8*, 1182–1188.
123. Lu, J.; Chen, Y.; Wen, X.; Wu, L.M.; Jia, X.; Liu, Y.C.; Liu, Z.L.  $^{14}\text{N}/^{15}\text{N}$  and  $^{12}\text{C}/^{13}\text{C}$  Equilibrium isotope effects on the Eelectron-transfer reaction between *N*-methylphenothiazine and its radical cation. *J. Phys. Chem. A* **1999**, *103*, 6998–7007. [[CrossRef](#)]
124. Rathore, R.; Burns, C.L.; Deselnicu, M.I. Multiple-electron transfer in a single step. Design and synthesis of highly charged cation-radical salts. *Org. Lett.* **2001**, *18*, 2887–2890. [[CrossRef](#)]
125. Hiraoka, S.; Okamoto, T.; Kozaki, M.; Shiomi, D.; Sato, K.; Takui, T.; Okada, K. A stable radical-substituted radical cation with strongly ferromagnetic interaction: Nitronyl nitroxide-substituted 5,10-diphenyl-5,10-dihydrophenazine radical cation. *J. Am. Chem. Soc.* **2004**, *126*, 58–59. [[CrossRef](#)] [[PubMed](#)]
126. Shorafa, H.; Mollenhauer, D.; Paulus, B.; Seppelt, K. The Two Structures of the Hexafluorobenzene Radical Cation  $\text{C}_6\text{F}_6^{\bullet+}$ . *Angew. Chem. Int. Ed.* **2009**, *48*, 5845–5847. [[CrossRef](#)] [[PubMed](#)]
127. Back, O.; Donnadiou, B.; Parameswaran, P.; Frenking, G.; Bertrand, G. Isolation of crystalline carbene-stabilized  $\text{P}_2$ -radical cations and  $\text{P}_2$ -dications. *Nat. Chem.* **2010**, *2*, 369–373. [[CrossRef](#)] [[PubMed](#)]
128. Chen, X.; Wang, X.; Zhou, Z.; Li, Y.; Sui, Y.; Ma, J.; Wang, X.; Power, P.P. Reversible  $\sigma$ -dimerizations of persistent organic radical cations. *Angew. Chem. Int. Ed.* **2013**, *52*, 589–592. [[CrossRef](#)] [[PubMed](#)]
129. Kumar, S.; Ajayakumar, M.R.; Hundal, G.; Mukhopadhyay, P. Extraordinary stability of naphthalenediimider Ion and its ultra-electron-deficient precursor: Strategic role of the phosphonium group. *J. Am. Chem. Soc.* **2014**, *136*, 12004–12010. [[CrossRef](#)] [[PubMed](#)]
130. Welker, E.A.; Tiley, B.L.; Sasaran, C.M.; Zuchero, M.A.; Tong, W.S.; Vettleson, M.J.; Richards, R.A.; Geruntho, J.J.; Stoll, S.; Wolbach, J.P.; et al. Conformational change with steric interactions affects the inner sphere component of concerted proton–electron transfer in a pyridyl-appended radical cation system. *J. Org. Chem.* **2015**, *80*, 8705–8712. [[CrossRef](#)] [[PubMed](#)]
131. Kayahara, E.; Kouyama, T.; Kato, T.; Yamago, S. Synthesis and characterization of [n]CPP (n = 5, 6, 8, 10, and 12) radical cation and dications: Size-dependent absorption, spin, and charge delocalization. *J. Am. Chem. Soc.* **2016**, *138*, 338–344. [[CrossRef](#)] [[PubMed](#)]
132. Peters, S.J.; Turk, M.R.; Kiesewetter, M.K.; Reiter, R.C.; Stevenson, C.D. The cyclooctatriene- $\eta^2$ -ynyl potassium zwitterionic radical: Evidence for a potassium organometallic. *J. Am. Chem. Soc.* **2003**, *125*, 11212–11213. [[CrossRef](#)] [[PubMed](#)]
133. Yi, C.; Blum, C.; Liu, S.-X.; Keene, T.D.; Frei, G.; Neels, A.; Decurtins, S. Isolable Zwitterionic Pyridinio-semiquinone  $\pi$ -Radicals. Mild and Efficient Single-Step Access to Stable Radicals. *Org. Lett.* **2009**, *11*, 2261–2262. [[CrossRef](#)] [[PubMed](#)]
134. Yong, G.P.; Li, C.F.; Li, Y.Z.; Luo, S.W. New zwitterionic radical salts: Dimers in solution and unusual magnetic and luminescent properties in the solid state. *Chem. Commun.* **2010**, *46*, 3194–3196. [[CrossRef](#)] [[PubMed](#)]

135. Sanna, E.; Martinez, L.; Rotger, C.; Blasco, S.; Gonzalez, J.; Espana, G.E.; Costa, A. Squaramide-based reagent for selective chromogenic sensing of Cu(II) through a zwitterion radical. *Org. Lett.* **2010**, *12*, 3840–3843. [[CrossRef](#)] [[PubMed](#)]
136. Schmidt, D.; Bialas, D.; Wurthner, F. Ambient stable zwitterionic perylene bisimide-centered radical. *Angew. Chem. Int. Ed.* **2015**, *54*, 3611–3614. [[CrossRef](#)] [[PubMed](#)]
137. Huang, J.; Sumpter, B.G.; Meunier, V.; Tian, Y.H.; Kertesz, M. Cyclo-biphenalenyl biradicaloid molecular materials: Conformation, tautomerization, magnetism, and thermochromism. *Chem. Mater.* **2011**, *23*, 874–885. [[CrossRef](#)]
138. Bag, P.; Pal, S.K.; Itkis, M.E.; Sarkar, A.; Tham, F.S.; Donnadiou, B.; Haddon, R.C. Synthesis of tetrachalcogenide-substituted phenalenyl derivatives: Preparation and solid-state characterization of bis(3,4,6,7-tetrathioalkyl-phenalenyl) boron radicals. *J. Am. Chem. Soc.* **2013**, *135*, 12936–12939. [[CrossRef](#)] [[PubMed](#)]
139. Aboaku, S.; Filho, A.P.; Bindilatti, V.; Oliveira, N.F.; Schlueter, J.A., Jr.; Lahti, P.M. Aminophenylnitronyl nitroxides: Highly networked hydrogen-bond assembly in organic radical materials. *Chem. Mater.* **2011**, *23*, 4844–4856. [[CrossRef](#)]
140. Seber, G.; Freitas, R.S.; Oliveira, N.F.; Schlueter, J.A., Jr.; Lahti, P.M. Crystal packing and magnetism in phenolic nitronyl nitroxides: 2-(3',5'-dimethoxy-4'-hydroxyphenyl)-4,4,5,5-tetramethyl-4,5-dihydro-1H-imidazole-1-oxyl. *Cryst. Growth Des.* **2013**, *13*, 893–900. [[CrossRef](#)]
141. Mostovich, E.A.; Borozdina, Y.; Enkelmann, V.; Langer, K.R.; Wolf, B.; Lang, M.; Baumgarten, M. Planar biphenyl-bridged biradicals as building blocks for the design of quantum magnets. *Cryst. Growth Des.* **2012**, *12*, 54–59. [[CrossRef](#)]
142. Constantinides, C.P.; Berezin, A.A.; Manoli, M.; Leitus, G.M.; Zissimou, G.A.; Bendikov, M.; Rawson, J.M.; Koutentis, P.A. Structural, Magnetic, and Computational Correlations of Some Imidazolo-Fused 1,2,4-Benzotriazinyl Radicals. *Chem. Eur. J.* **2014**, *20*, 5388–5396. [[CrossRef](#)] [[PubMed](#)]
143. Constantinides, C.P.; Koutentis, P.A.; Rawson, J.M. Antiferromagnetic interactions in 1D heisenberg linear chains of 7-(4-fluorophenyl) and 7-phenyl-substituted 1,3-diphenyl-1,4-dihydro-1,2,4-benzotriazin-4-yl radicals. *Chem. Eur. J.* **2012**, *18*, 15433–15438. [[CrossRef](#)] [[PubMed](#)]
144. Constantinides, C.P.; Koutentis, P.A.; Rawson, J.M. Ferromagnetic interactions in a 1D alternating linear chain of p-stacked 1,3-diphenyl-7-(thien-2-yl)-1,4-dihydro-1,2,4-benzotriazin-4-yl radicals. *Chem. Eur. J.* **2012**, *18*, 7109–7116. [[CrossRef](#)] [[PubMed](#)]
145. Constantinides, C.P.; Carter, E.; Murphy, D.M.; Manoli, M.; Leitus, G.M.; Bendikov, M.; Rawson, J.M.; Koutentis, P.A. Spin-triplet excitons in 1,3-diphenyl-7-(fur-2-yl)-1,4-dihydro-1,2,4-benzotriazin-4-yl. *Chem. Commun.* **2013**, *49*, 8662–8664. [[CrossRef](#)] [[PubMed](#)]
146. Yan, B.; Cramen, J.; McDonald, R.; Frank, N.L. Ferromagnetic spin-delocalized electron donors for multifunctional materials: P-conjugated benzotriazinyl radicals. *Chem. Commun.* **2011**, *47*, 3201–3203. [[CrossRef](#)] [[PubMed](#)]
147. Constantinides, C.P.; Berezin, A.A.; Zissimou, G.A.; Manoli, M.; Leitus, G.M.; Bendikov, M.; Probert, M.R.; Rawson, J.M.; Koutentis, P.A. A Magnetostructural investigation of an abrupt spin transition for 1-Phenyl-3-trifluoromethyl-1,4-dihydrobenzo[e][1,2,4]triazin-4-yl. *J. Am. Chem. Soc.* **2014**, *136*, 11906–11909. [[CrossRef](#)] [[PubMed](#)]
148. Ciccullo, F.; Gallagher, N.M.; Geladari, O.; Chassé, T.; Rajca, A.; Casu, M.B. A Derivative of the Blatter Radical as a Potential Metal-Free Magnet for Stable Thin Films and Interfaces. *ACS Appl. Mater. Interfaces* **2016**, *8*, 1805–1812. [[CrossRef](#)] [[PubMed](#)]
149. Winter, S.M.; Datta, S.; Hill, S.; Oakley, R.T. Magnetic anisotropy in a heavy atom radical ferromagnet. *J. Am. Chem. Soc.* **2011**, *133*, 8126–8129. [[CrossRef](#)] [[PubMed](#)]
150. Yu, X.; Mailman, A.; Lakin, K.; Assoud, A.; Robertson, C.M.; Noll, B.C.; Campana, C.F.; Howard, J.A.K.; Dube, P.A.; Oakley, R.T. Semiquinone-bridged bisdithiazolyl radicals as neutral radical conductors. *J. Am. Chem. Soc.* **2012**, *134*, 2264–2275. [[CrossRef](#)] [[PubMed](#)]
151. Yu, X.; Mailman, A.; Dube, P.A.; Assoud, A.; Oakley, R.T. The first semiquinone-bridged bisdithiazolyl radical conductor: A canted antiferromagnet displaying a spin-flop transition. *Chem. Commun.* **2011**, *47*, 4655–4657. [[CrossRef](#)] [[PubMed](#)]

152. Mailman, A.; Winter, S.M.; Wong, J.W.L.; Robertson, C.M.; Assoud, A.; Dube, P.A.; Oakley, R.T. Multiple orbital effects and magnetic ordering in a neutral radical. *J. Am. Chem. Soc.* **2015**, *137*, 1044–1047. [[CrossRef](#)] [[PubMed](#)]
153. Rajca, A.; Olankitwanit, A.; Wang, Y.; Boratynski, P.J.; Pink, M.; Rajca, S. High-spin  $S = 2$  ground state aminyl tetraradicals. *J. Am. Chem. Soc.* **2013**, *135*, 18205–18215. [[CrossRef](#)] [[PubMed](#)]
154. Ueda, A.; Yamada, S.; Isono, T.; Kamo, H.; Nakao, A.; Kumai, R.; Nakao, H.; Murakami, Y.; Yamamoto, K.; Nishio, Y.; et al. Hydrogen-bond-dynamics-based switching of conductivity and magnetism: A phase transition caused by deuterium and electron transfer in a hydrogen-bonded purely organic conductor crystal. *J. Am. Chem. Soc.* **2014**, *136*, 12184–12192. [[CrossRef](#)] [[PubMed](#)]
155. Zeng, Z.; Sung, Y.M.; Bao, N.; Tan, D.; Lee, R.; Zafra, J.L.; Lee, B.S.; Ishida, M.; Ding, J.; Navarrete, J.T.L.; et al. Stable Tetrabenzo-Chichibabin's hydrocarbons: Tunable ground state and unusual transition between their closed-shell and open-shell resonance forms. *J. Am. Chem. Soc.* **2012**, *134*, 14513–14525. [[CrossRef](#)] [[PubMed](#)]
156. Sun, Z.; Huang, K.W.; Wu, J. Soluble and stable heptazethrenebis(dicarboximide) with a singlet open-shell ground state. *J. Am. Chem. Soc.* **2011**, *133*, 11896–11899. [[CrossRef](#)] [[PubMed](#)]
157. Li, Y.; Heng, W.K.; Lee, B.S.; Aratani, N.; Zafra, J.L.; Bao, N.; Lee, R.; Sung, Y.M.; Sun, Z.; Huang, K.W.; et al. Kinetically blocked stable heptazethrene and octazethrene: Closed-shell or open-shell in the ground state? *J. Am. Chem. Soc.* **2012**, *134*, 14913–14922. [[CrossRef](#)] [[PubMed](#)]
158. Sun, Z.; Lee, S.; Park, K.H.; Zhu, X.; Zhang, W.; Zheng, B.; Hu, P.; Zeng, Z.; Das, S.; Li, Y.; et al. Dibenzohaptazethrene isomers with different biradical characters: An exercise of Clar's aromatic sextet rule in singlet biradicaloids. *J. Am. Chem. Soc.* **2013**, *135*, 18229–18236. [[CrossRef](#)] [[PubMed](#)]
159. Zeng, Z.; Ishida, M.; Zafra, J.L.; Zhu, X.; Sung, Y.M.; Bao, N.; Webster, R.D.; Lee, B.S.; Li, R.W.; Zeng, W.; et al. Pushing extended p-quinodimethanes to the limit: Stable tetracyano-oligo(N-annulated perylene) quinodimethanes with tunable ground states. *J. Am. Chem. Soc.* **2013**, *135*, 6363–6371. [[CrossRef](#)] [[PubMed](#)]
160. Hu, P.; Lee, S.; Heng, T.S.; Aratani, N.; Goncalves, T.P.; Qi, Q.; Shi, X.; Yamada, H.; Huang, K.W.; Ding, J.; et al. Toward tetraradicaloid: The effect of fusion mode on radical character and chemical reactivity. *J. Am. Chem. Soc.* **2016**, *138*, 1065–1077. [[CrossRef](#)] [[PubMed](#)]
161. Huang, R.; Phan, H.; Heng, T.S.; Hu, P.; Zeng, W.; Dong, S.Q.; Das, S.; Shen, Y.; Ding, J.; Casanova, D.; et al. Higher order  $\pi$ -conjugated polycyclic hydrocarbons with open-shell singlet ground state: Nonazethrene versus nonacene. *J. Am. Chem. Soc.* **2016**, *138*, 10323–10330. [[CrossRef](#)] [[PubMed](#)]
162. Das, S.; Heng, T.S.; Zafra, J.L.; Burrezo, P.M.; Kitano, M.; Ishida, M.; Gopalakrishna, T.Y.; Hu, P.; Osuka, A.; Casado, J.; et al. Fully fused quinoidal/aromatic carbazole macrocycles with polyradical characters. *J. Am. Chem. Soc.* **2016**, *138*, 7782–7790. [[CrossRef](#)] [[PubMed](#)]
163. Nishide, H.; Oyaizu, K. Toward Flexible Batteries. *Science* **2008**, *319*, 737–738. [[CrossRef](#)] [[PubMed](#)]
164. Morita, Y.; Suzuki, S.; Sato, K.; Takui, T. Synthetic organic spin chemistry for structurally well-defined open-shell graphene fragments. *Nat. Chem.* **2011**, *3*, 197–204. [[CrossRef](#)] [[PubMed](#)]
165. Yoshino, T.; Nishida, S.; Sato, K.; Nakazawa, S.; Rahimi, R.D.; Toyota, K.; Shiomi, D.; Morita, Y.; Kitagawa, M.; Takui, T. ESR and  $^1\text{H}$ - $^{19}\text{F}$ -ENDOR/TRIPLE Study of Fluorinated Diphenylnitroxides as Synthetic Bus Spin-Qubit Radicals with Client Qubits in Solution. *J. Phys. Chem. Lett.* **2011**, *2*, 449–453. [[CrossRef](#)]
166. Ajayakumar, M.R.; Mukhopadhyay, P. Naphthalene-bis-hydrazimide: Radical Anions and ICT as New Bimodal Probes for Differential Sensing of a Library of Amines. *Chem. Commun.* **2009**, 3702–3704. [[CrossRef](#)] [[PubMed](#)]
167. Ajayakumar, M.R.; Yadav, S.; Ghosh, S.; Mukhopadhyay, P. Single-Electron Transfer Driven Cyanide Sensing: A New Multimodal Approach. *Org. Lett.* **2010**, *46*, 2646–2649. [[CrossRef](#)] [[PubMed](#)]
168. Ajayakumar, M.R.; Mandal, K.; Rawat, K.; Asthana, D.; Pandey, R.; Sharma, A.; Yadav, S.; Ghosh, S.; Mukhopadhyay, P. Single Electron Transfer-Driven Multi-Dimensional Signal Read-out Function of TCNQ as an "Off-the-Shelf" Detector for Cyanide. *ACS Appl. Mater. Interfaces* **2013**, *5*, 6996–7000. [[CrossRef](#)] [[PubMed](#)]

